When Altruism Meets Autonomy: Managing Bottleneck Congestion with Strategic Autonomous Vehicles

Kexin Wang[1], Haohui He[1], and Ruolin Li*[1]

[1] *Department of Civil and Environmental Engineering, University of Southern California*

kwang255@usc.edu, haohuihe@usc.edu, ruolinl@usc.edu

Abstract

Weaving ramps are critical bottlenecks in highway networks due to conflicting traffic flows and complex interactions among heterogeneous vehicle types. In mixed-autonomy settings, the presence of controllable autonomous vehicles (AVs) introduces new opportunities to influence system-level outcomes, yet the *structural* impact of such control remains poorly understood. This paper develops a unified equilibrium framework to capture, predict, and optimize aggregate lane-choice behavior in weaving ramps with heterogeneous vehicle populations. We first formulate a Wardrop-based model capturing the selfish behavior of human-driven vehicles (HDVs) and establish existence, uniqueness and validity of the resulting equilibrium. We then introduce a Stackelberg–Wardrop formulation in which AVs act as strategic leaders optimizing system performance, while HDVs respond through equilibrium adaptation. The framework is further generalized to incorporate HDVs' and AVs' heterogeneous behavioral preferences via a Social Value Orientation (SVO) model. Our analysis reveals a fundamental structural property of mixed-autonomy traffic systems: under selfish HDV behavior, the impact of AV penetration is inherently non-increasing, exhibiting plateau regions where performance remains unchanged and improves only at critical thresholds. These results provide principled guidance for the design of AV control and incentive mechanisms in the presence of selfish human behavior, and demonstrate how strategically controlled autonomous agents can be deployed to induce system-level efficiency gains in mixed-autonomy transportation networks.

1 Introduction

Mixed-autonomy traffic systems, in which autonomous vehicles (AVs) coexist with human-driven vehicles (HDVs), are expected to fundamentally reshape transportation networks (Talebpour and Mahmassani, 2016; Wu et al., 2017). A key distinction between these vehicle types lies in their decision-making capabilities: while HDVs act selfishly based on local information, AVs can be centrally coordinated and strategically controlled (Zhang and Nie, 2018; Ao et al., 2024). This asymmetry creates new opportunities to influence traffic equilibria and improve system performance. However, a fundamental question remains: how does the introduction of strategically controlled

agents alter equilibrium outcomes in systems dominated by selfish users? Addressing this question is a central challenge in transportation science and the focus of this paper. Highway weaving ramps provide a representative bottleneck setting in which such interactions are especially pronounced (Marczak et al., 2015; Chen and Ahn, 2018; Lee and Cassidy, 2008). Motivated by this setting, we study the strategic interplay between HDVs and AVs at weaving ramp bottlenecks, and examine how these interactions can inform the design of AV control policies.

We next motivate our problem setting from two complementary perspectives, mixed-autonomy systems and bottleneck characteristics at highway weaving ramps, before presenting our contributions.

1.1 Challenge of Mixed-Autonomy Systems

Mixed-autonomy systems, characterized by the coexistence of AVs and HDVs, introduce a fundamental shift in how traffic systems operate. Unlike traditional settings composed solely of human drivers (Beckmann et al., 1956; Roughgarden and Tardos, 2002), these systems feature a heterogeneous population with distinct decision-making mechanisms: HDVs act selfishly based on local information, while AVs can be algorithmically controlled and coordinated at the system level (Chen et al., 2017b). This asymmetry creates the potential to influence traffic equilibria through the strategic deployment and control of AVs.

Existing studies have demonstrated that AVs can improve traffic efficiency, enhance stability, and enable new forms of coordinated control, even at moderate penetration levels (Vinitsky et al., 2018; Wu et al., 2023). These benefits arise from the ability of AVs to implement system-level objectives, such as throughput maximization and congestion mitigation, which are typically beyond the scope of selfish human drivers. As a result, AVs can act as controllable agents that reshape traffic dynamics and influence the behavior of surrounding vehicles.

However, the effectiveness of such control critically depends on the interaction between AVs and HDVs (Lazar et al., 2017; Guo et al., 2022). When AV penetration is low, the system remains dominated by selfish HDV behavior, which may limit or even neutralize the impact of strategically controlled AVs (Lazar et al., 2018). As penetration increases, AVs gain greater influence over the aggregate traffic state, enabling more effective coordination and system-level improvements (Lioris et al., 2017; Guo and Ma, 2020). This suggests that the relationship between AV penetration and system performance is inherently nontrivial and mediated by equilibrium responses of HDVs, and also outlines a remaining fundamental gap: existing work largely focuses on performance improvements under specific control policies or simulation settings (Vinitsky et al., 2018; Zhang and Nie, 2018), but lacks a structural understanding of how strategically controlled AVs alter equilibrium outcomes in the presence of selfish users. In particular, it remains unclear how system performance evolves as AV penetration increases, and how behavioral heterogeneity shapes these dynamics. Addressing this gap requires a unified framework that captures the strategic interaction between controllable AVs and selfish HDVs at equilibrium. This motivates the development of the equilibrium-based models proposed in this paper.

1.2 Challenge of Highway Weaving Ramp

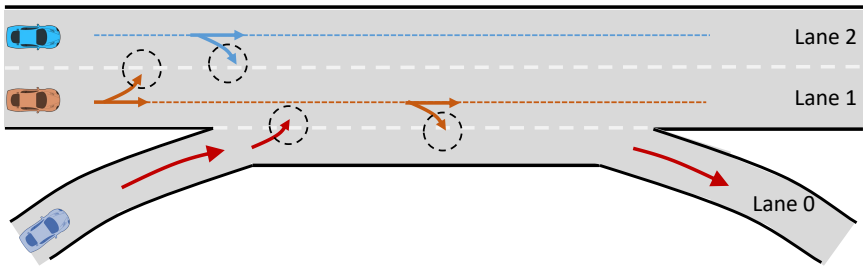

Figure 1: A highway weaving ramp example, which shows complex interactions between entering, exiting and going through vehicles.

The interaction between AVs and HDVs becomes particularly pronounced in localized bottleneck settings, where vehicles must make rapid and strategic decisions under strong spatial and temporal constraints. Examples include intersections (Dresner and Stone, 2008), roundabouts (Rodrigues et al., 2018), and highway merging, diverging, and weaving segments (Chandra and Manocha, 2022). In such environments, vehicles continuously adjust their behaviors, including merging, yielding, and changing lanes, in response to surrounding traffic conditions, leading to complex and highly coupled interactions.

Among these scenarios, highway weaving ramps provide a representative and analytically tractable bottleneck setting. In a typical configuration (Fig. 1), entering, exiting, and through vehicles must complete conflicting maneuvers within a limited roadway segment. This induces strong competition for space and priority: entering vehicles merge into the mainline, exiting vehicles traverse across lanes to reach the off-ramp, and through vehicles must decide whether to remain in their current lane or bypass congestion by changing lanes. These interdependent decisions generate substantial friction in traffic flow, leading to capacity reductions and congestion (Laval and Daganzo, 2006).

From a modeling perspective, weaving ramps naturally give rise to a strategic lane-choice problem (Marczak et al., 2015; Lee and Cassidy, 2008; Li et al., 2020a). In particular, a subset of vehicles, namely those traveling through the weaving segment, face a fundamental trade-off between remaining in a congested lane or switching lanes to avoid conflicts, while incurring maneuvering costs (Toledo et al., 2003; Kita, 1999; Kita et al., 2002). This trade-off is inherently strategic, as the cost of each decision depends on the aggregate behavior of other vehicles. Moreover, in mixed-autonomy settings, AVs can influence these decisions through coordinated control, while HDVs respond selfishly based on observed conditions (Talebpour and Mahmassani, 2016).

These features make weaving ramps an ideal setting to study how strategically controlled AVs interact with selfish HDVs and how such interactions shape equilibrium outcomes. At the same time, the strong coupling between merging and lane-changing behaviors amplifies congestion externalities, making it particularly challenging to design control strategies that achieve system-level improvements. This motivates the development of an equilibrium-based framework to analyze and manage lane-choice behavior in mixed-autonomy weaving bottlenecks.

1.3 Our contributions

This paper addresses the above question through the study of aggregate lane-choice behavior in highway weaving ramps. We develop a macroscopic game-theoretic framework that integrates (i) selfish HDV behavior modeled via Wardrop equilibrium, (ii) strategic AV control modeled through a Stackelberg formulation, and (iii) heterogeneous behavioral preferences captured using a Social Value Orientation (SVO) model.

Our analysis reveals a fundamental structural property of mixed-autonomy traffic systems. As AV penetration increases, system performance is not strictly improving; instead, the social cost follows a piecewise-constant regime structure, remaining unchanged over intervals of penetration and decreasing only at critical thresholds. Each regime is governed by a unique active behavioral type, and behavioral heterogeneity reshapes these thresholds, thereby altering the timing and magnitude of system-level improvements.

These findings suggest that mixed-autonomy traffic systems should not be viewed as smooth transitions from human-driven to fully automated operation. Rather, they exhibit regime-switching behavior driven by the interaction between strategic control and heterogeneous preferences. This perspective provides a new lens for understanding congestion dynamics and informs the design of AV deployment and control policies.

The main contributions of this study are as follows:

- **Equilibrium Framework for Mixed Autonomy:** We develop a unified equilibrium framework for lane-choice behavior in weaving ramps, integrating Wardrop equilibrium for HDVs with Stackelberg control of AVs, and extending to heterogeneous populations via SVO-based preferences.
- **Existence, Uniqueness, and Structural Characterization:** We establish existence and uniqueness of the baseline selfish HDV equilibrium and characterize how mixed-autonomy equilibrium outcomes depend on traffic composition and control inputs.
- **Implications for AV Control Design:** We provide actionable insights for the design of AV control and incentive mechanisms, including conditions under which AV deployment leads to measurable reductions in system-level delay.

2 Related Works

We next review the relevant literature along two key dimensions: models of lane-changing behavior and game-theoretic frameworks for analyzing strategic interactions in mixed-autonomy traffic systems.

2.1 Lane-Changing Behavior in Mixed Autonomy

Lane-changing is a critical maneuver in traffic flow, as improper lane changes can create voids that trigger stop-and-go oscillations or even lead to breakdowns near bottlenecks (Laval and Leclercq, 2008). Empirical evidence suggest that approximately 10% of crashes are attributable to lane-changing behavior (Ji and Levinson, 2020), underscoring the need for improved models of lane choice. Over the past decades, a variety of microscopic lane-changing models have been developed to describe when and how drivers decide to change lanes. Early rule-based frameworks, such as Gipps' seminal model (Gipps, 1986), formalized drivers' decision processes based on safe distance and collision risk criteria. Later studies refined gap-acceptance logic by distinguishing free, cooperative, and forced maneuvers depending on urgency and driver willingness to decelerate (Hidas, 2002). These classical models, along with subsequent works (Sun and Elefteriadou, 2010; Li et al., 2019, 2020b), established the foundation for simulating both mandatory and discretionary lane changes under human driving conditions.

With the advent of AVs, research has begun to examine how partial automation may influence lane-changing dynamics and be leveraged to improve traffic performance (Ghiasi et al., 2017). Data-driven approaches, particularly reinforcement learning, have been applied to train autonomous agents to replicate or optimize human-like lane-change decisions (Shalev-Shwartz et al., 2016; Wang et al., 2019). Notably, studies show that even a small fraction of AVs can affect traffic conditions. For example, with 5-10% AV penetration, properly designed AV control policies were found to increase average speeds and suppress stop-and-go waves in simulations (Wang et al., 2020). Field experiments further demonstrate the potential of cooperative lane-changing (Du et al., 2020; Fan et al., 2025), where prototype AVs successfully executed coordinated lane maneuvers in live traffic, assisting HDVs during merges (Adebisi et al., 2020). Other system-wide analyses similarly confirm that AV deployment can improve efficiency and stability (Li et al., 2018; Guo et al., 2021). These findings illustrate that autonomy and V2X connectivity have powerful potential to reduce disturbances and enhance throughput during lane changes.

Furthermore, highway weaving ramps present a particular challenging context for lane-changing in mixed autonomy. Weaving ramps are recognized as capacity bottlenecks, with throughput reductions of 3-20% once congestion sets (Yan et al., 2024). Traditional studies attribute this "capacity drop" to human behavioral factors, including suboptimal gap acceptance and the spatial distribution of lane changes (Cassidy and Bertini, 1999; Treiber and Kesting, 2013). AVs, by contrast, create opportunities for predictive and cooperative maneuvering: equipped with connectivity, they can act on a system level, unlike HDVs limited by perception and independent decision-making (Talebpour and Mahmassani, 2016; Stern et al., 2018). Recent research has thus proposed coordinated lane-changing control for weaving ramps, where centralized or distributed algorithms optimize lane-change trajectories across multiple vehicles (Rios-Torres and Malikopoulos, 2016). While promising in fully automated scenarios, these methods often require solving large-scale optimization problems and encounter scalability issues as vehicle numbers increase (Zhou et al., 2016; Chen et al., 2017a). Moreover, many assume high AV penetration and overlook the ongoing transition phase with mixed

fleets (Shladover et al., 2012). In summary, existing studies have largely focused either on localized, lane-changing decisions or on centralized coordination under idealized conditions, leaving a gap in modeling aggregate lane-choice behavior in weaving ramps that accounts for the strategic interplay between AVs and HDVs. To address this, our work introduces a set of game-theoretic formulations for lane choices in mixed-autonomy weaving zones.

2.2 Game-Theoretic Modeling in Mixed Autonomy

Game-theoretic frameworks have proven well-suited for studying mixed-autonomy environments, as they can capture interactive behaviors among heterogeneous agents within a unified decision-making model. By accommodating diverse objectives in a single framework, game theory enables a rigorous analysis of strategic decision-making in these complex settings. For instance, Li et al. (2023) formulated a Nash equilibrium approach to AV lane-changing that explicitly balances safety and energy efficiency. Similarly, Lopez et al. (2022) combined normal-form game formulations, Nash equilibrium analysis, and Q-learning techniques to improve the stability of multi-agent lane-changing decisions. In another study, Talebpour et al. (2015) employed a fictitious play-based framework to model AV lane-changing in a V2V communication-enabled environment, where drivers iteratively update their beliefs and compute best responses. Together, these studies demonstrate the effectiveness of game-theoretic methods for capturing realistic and strategic interactions among vehicles in mixed traffic.

Beyond modeling individual driver behaviors, game-theoretic principles also facilitate system-level traffic analysis. Wardrop's first principle formalizes the notion of a user-equilibrium traffic flow, wherein no driver can reduce their travel time by unilaterally changing behaviors (Wardrop, 1952). While microscopic behavioral models are critical for operational-level decision making, aggregate equilibrium-based approaches provide valuable insights for high-level planning and policy design by transportation agencies and companies. In fact, such equilibrium conditions are often integrated into bi-level models (Chiou, 2005). These formulations often referred to as mathematical programs with equilibrium constraints, offer a principled framework for analyzing system-optimal strategies under rational user responses.

In our prior work, we developed several game-theoretic frameworks to capture aggregate lane-choice behavior in specific traffic scenarios. For example, one study considered a highway diverge with bifurcating lanes, where vehicles must split into two downstream links (Li et al., 2019), while another examined lane choice at highway on-ramps, where merging vehicles interact with mainline traffic (Li et al., 2020b, 2021). These models were shown to effectively capture and predict HDVs' lane-choice behavior in their respective settings. Building on these foundations, the present work significantly extends the scope and depth of the analysis. We move beyond homogeneous, single-scenario models to a unified framework that incorporates mixed autonomy, strategic AV control, and heterogeneous behavioral preferences. This extension enables us to characterize how equilibrium structure evolves under the interaction between controllable and selfish agents, which is not captured in prior models.

3 Problem Setting: Weaving Ramps

In this section, we introduce our core scenario, highway weaving ramps, defined as freeway segments where an on-ramp and an off-ramp are located in close proximity, forcing entering, exiting, and through vehicles to perform intensive lane-changing maneuvers within a short distance (Transportation Research Board, 2010). We first examine the inherent interaction complexity of such facilities, identify key lane-choice behaviors, and then define the essential notations for our framework. To maintain clarity, we focus on a representative case with two mainline lanes, as illustrated in Figure 1.

3.1 Key Strategic Lane Choice Behavior

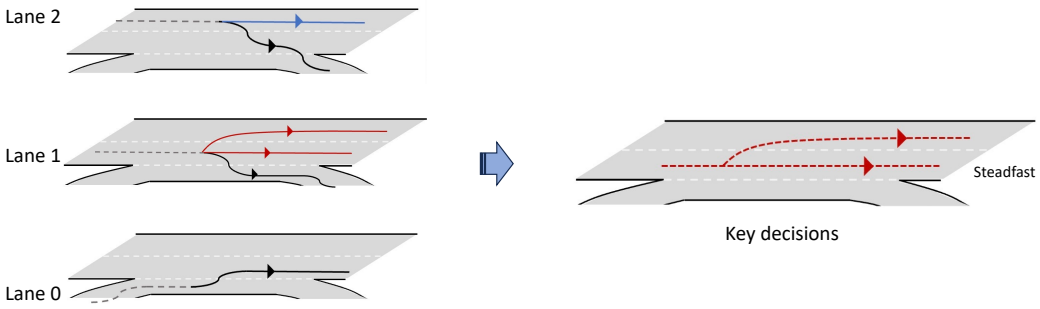

Figure 2: This figure illustrates the structure of lane-changing decisions within a highway weaving ramp. The flows shown in black represent entering and exiting vehicles, along with through vehicles in the inner mainline lane (Lane 2), whose decisions are predetermined by their initial intentions or by the absence of lane-changing incentives, and are not subject to strategic adjustment. By contrast, the flows shown in red correspond to through vehicles in the outer mainline lane (Lane 1), which retain the flexibility to modify their lane-changing decisions in response to system-level delays and thus constitute the focus of our analysis.

Most vehicles in this setting operate under predefined goal constraints. As illustrated in Figure 1, entering vehicles on Lane 0 must merge into Lane 1 to access the highway, while exiting vehicles on Lane 1 and 2 must leave via the weaving ramp. Through vehicles in Lane 2 have no incentive to change lanes. Consequently, their lane-changing decisions are relatively rigid and less responsive to external control strategies.

By contrast, through vehicles in Lane 1 represent a distinct class with more flexible objectives and greater susceptibility to external influence. These vehicles face two strategic decisions: (1) **steadfast in Lane 1**, accepting potential interactions and disruptions from both entering and exiting flows, or (2) **bypass to Lane 2** to avoid the conflict zone, while incurring the risks and time costs associated with lane changes. These decisions reflect a trade-off between exposure to disruption and the effort of maneuvering.

Strategic decision-making also differs substantially between AVs and HDVs. HDV behavior is largely spontaneous and difficult to influence, particularly in short-horizon scenarios such as weaving

ramps, where decisions must be made almost instantaneously. By contrast, AVs are more controllable, because they can access richer information and execute timely decisions. This controllability suggests that, as AV penetration increases in the near future, their decision-making can be leveraged to improve traffic system performance. Given this behavioral heterogeneity, our analysis focuses on how AVs make strategic decisions to regulate traffic flow and how HDVs respond selfishly to those decisions in Lane 1. In particular, we investigate how such interactions generate distinct behavioral patterns and evaluate their implications for both individual outcomes and system-level delays, which constitutes the central focus of this study.

3.2 Notations

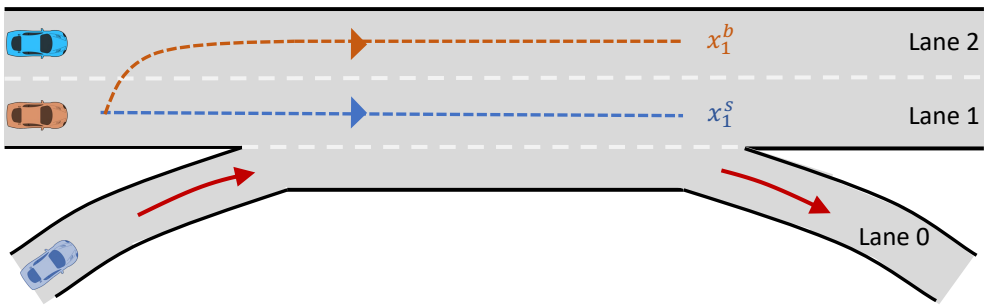

Figure 3: The highway weaving ramp consists of three lanes. Lane 0 accommodates the entering flow f_0^{enter}, and Lane 2 carries both the exiting flow f_2^{exit} and the non-strategic through flow f_2^{s}. These flows are treated as given parameters. By contrast, Lane 1 contains two through flows f_1^{s}(steadfast) and f_1^{b}(bypass), which constitute the key decision variables in this study.

To evaluate the impact of strategic vehicle behavior on system performance and capture interactions among heterogeneous vehicle types, we adopt a macroscopic modeling perspective. Our focus is on the aggregate traffic flow patterns of each vehicle type, rather than the microscopic actions of individual vehicles.

The vehicle types considered and their corresponding flow notations are as follows: (1) f_0^{enter}: entering vehicles on Lane 0 that merge into Lane 1; (2) f_2^{exit}: exiting vehicles on Lane 2 that traverse Lane 1 and exit the weaving ramp via Lane 0; (3) f_2^{s}: through vehicles on Lane 2; (4) f_1^{s}: through vehicles on Lane 1 that remain steadfast; (5) f_1^{b}: through vehicles on Lane 1 that bypass to Lane 2. Since our focus is on flows whose decisions can be strategically controlled, we distinguish between predetermined behaviors and strategic choices. Vehicle types (1)-(3) are goal-constrained, with actions either predetermined or lacking incentives for adjustment, and are therefore treated as **exogenous normalized flow ratios**. By contrast, vehicle types (4) and (5) represent decision-dependent variables whose allocations adapt to traffic conditions or control policies, and are modeled as **decision-dependent normalized flow ratios**.

The *exogenous normalized flow ratios* are defined as follows:

$$n_0^{\text{enter}} := \frac{f_0^{\text{enter}}}{f_0^{\text{enter}} + f_2^{\text{exit}} + f_2^{\text{s}}}, \tag{1}$$

$$n_2^{\text{exit}} := \frac{f_2^{\text{exit}}}{f_0^{\text{enter}} + f_2^{\text{exit}} + f_2^{\text{s}}}, \tag{2}$$

$$n_2^{\text{s}} := \frac{f_2^{\text{s}}}{f_0^{\text{enter}} + f_2^{\text{exit}} + f_2^{\text{s}}}, \tag{3}$$

where we have $n_0^{\text{enter}} \geq 0, n_2^{\text{exit}} \geq 0, n_2^{\text{s}} \geq 0$, and naturally $n_0^{\text{enter}} + n_2^{\text{exit}} + n_2^{\text{s}} = 1$. The normalized flow ratios n_0^{enter}, n_2^{exit} and n_2^{s} represent the proportions of entering, exiting, and through vehicles relative to the total vehicle flow in the vicinity of Lane 1, originating from Lane 0 or Lane 2. These flow ratios are treated as known parameters in the model and are collectively denoted by the flow configuration vector $\mathbf{n} := \left(n_0^{\text{enter}}, n_2^{\text{exit}}, n_2^{\text{s}}\right)$.

The *decision-dependent normalized flow ratios* are defined separately as follows:

$$x_1^{\text{s}} := \frac{f_1^{\text{s}}}{f_1}, \tag{4}$$

$$x_1^{\text{b}} := \frac{f_1^{\text{b}}}{f_1}, \tag{5}$$

where naturally $x_1^{\text{s}} + x_1^{\text{b}} = 1$, $x_1^{\text{s}} \geq 0$, and $x_1^{\text{b}} \geq 0$. The variable x_1^{s} represents the proportion of steadfast vehicles on Lane 1, and x_1^{b} represents the proportion of bypassing vehicles on Lane 1.

We incorporate AVs into the decision-dependent flows through the penetration rate p, as these flows are directly influenced by strategic decision-making. While AVs could in principle be included in the exogenous normalized flows, such an extension is unlikely to yield meaningful improvements in overall system performance. Accordingly, we restrict AVs to the decision-dependent categories and exclude them from n_0^{enter}, n_2^{exit} and n_2^{s}. The total flow distribution vector is defined as $\mathbf{x} := (x_{1,\text{CAV}}^{\text{s}}, x_{1,\text{CAV}}^{\text{b}}, x_{1,\text{HDV}}^{\text{s}}, x_{1,\text{HDV}}^{\text{b}})$, where the aggregate decision-dependent flow ratios x_1^{s} and x_1^{b} are given by the sums of their AV and HDV components:

$$x_1^{\text{s}} = x_{1,\text{HDV}}^{\text{s}} + x_{1,\text{CAV}}^{\text{s}}, \tag{6}$$

$$x_1^{\text{b}} = x_{1,\text{HDV}}^{\text{b}} + x_{1,\text{CAV}}^{\text{b}}, \tag{7}$$

where we have $x_{1,\text{CAV}}^{\text{s}} + x_{1,\text{CAV}}^{\text{b}} = p$, and $x_{1,\text{HDV}}^{\text{s}} + x_{1,\text{HDV}}^{\text{b}} = 1 - p$.

The relationships defined above establish the notation and the decomposition of flows into AV and HDV components. In the subsequent sections, we first formulate a strategic lane choice model under the Wardrop equilibrium framework for an HDV-only environment. This framework is then extended to a bi-level Stackelberg-Wardrop formulation, in which **dedicated altruistic CAVs**, which are centrally controlled AVs with prescribed strategies, are introduced to manage and influence system-level behavior. Finally, the model is generalized to a mixed-traffic setting that incorporates **relaxed altruistic CAVs**, i.e., AVs whose behavior is guided by incentivization mechanisms rather

than direct control. All flow-ratio variables discussed in the remainder of the paper are defined with respect to this framework.

4 Selfish HDVs' Strategic Lane Choice Behavior as a Baseline

We begin by analyzing the decision-making process of HDVs in the absence of AVs, i.e., when the AV penetration rate $p = 0$ and $x^{\mathrm{s}}_{1,\mathrm{CAV}} = x^{\mathrm{b}}_{1,\mathrm{CAV}} = 0$. In this case, HDVs are assumed to behave selfishly, seeking to minimize their individual travel costs, primarily time delays, while navigating the weaving ramp. Such behavior can be effectively captured by the Wardrop equilibrium framework (Wardrop, 1952), which represents a state where no driver can unilaterally reduce travel time by changing lanes.

4.1 The Baseline Model Framework

In the highway weaving ramps, decision-making vehicles choose between two strategic behaviors: **steadfast behavior** associated with a cost $J^{\mathrm{s}}_1(\mathbf{x})$, and **bypassing behavior**, associated with a cost $J^{\mathrm{b}}_1(\mathbf{x})$. The Wardrop-based model captures the equilibrium relationship between the steadfast flow rates $x^{\mathrm{s}}_{1,\mathrm{HDV}}$, the bypassing flow rate $x^{\mathrm{b}}_{1,\mathrm{HDV}}$, and their corresponding delay costs $J^{\mathrm{s}}_1(\mathbf{x})$ and $J^{\mathrm{b}}_1(\mathbf{x})$. At the lane choice equilibrium, no vehicles have incentive to change their lanes.

Definition 1 (HDVs' Wardrop Lane Choice Equilibrium)**.** For a given weaving ramp configuration $G = (\mathbf{N}, \mathbf{C})$, a flow distribution vector $\mathbf{x} := (x^{\mathrm{s}}_{1,\mathrm{HDV}}, x^{\mathrm{b}}_{1,\mathrm{HDV}})$ is in equilibrium if and only if

$$x^{\mathrm{s}}_{1,\mathrm{HDV}}(J^{\mathrm{s}}_1(\mathbf{x}) - J^{\mathrm{b}}_1(\mathbf{x})) \leq 0, \tag{8a}$$

$$x^{\mathrm{b}}_{1,\mathrm{HDV}}(J^{\mathrm{b}}_1(\mathbf{x}) - J^{\mathrm{s}}_1(\mathbf{x})) \leq 0. \tag{8b}$$

This equilibrium model specifies that HDVs adopt the strategy that minimizes their own travel cost. Specifically, when bypassing incurs a lower cost ($J^{\mathrm{s}}_1(\mathbf{x}) - J^{\mathrm{b}}_1(\mathbf{x}) > 0$), all Lane 1 through vehicles choose to bypass, resulting in $x^{\mathrm{s}}_{1,\mathrm{HDV}} = 0$. Conversely, when steadfast travel is less costly ($J^{\mathrm{b}}_1(\mathbf{x}) - J^{\mathrm{s}}_1(\mathbf{x}) > 0$), all Lane 1 through vehicles remain in their lane, yielding $x^{\mathrm{b}}_{1,\mathrm{HDV}} = 0$. When the costs of the two strategies are equal ($J^{\mathrm{b}}_1(\mathbf{x}) - J^{\mathrm{s}}_1(\mathbf{x}) = 0$), both behaviors may coexist, producing nonzero values of x^{s}_1 and x^{b}_1. The resulting Wardrop equilibrium represents a long-term, steady-state distribution of strategies, which may not occur at every moment in real traffic but captures the aggregate outcome of repeated behavioral adjustments over time.

4.2 The Cost Model

To model the costs associated with the two lane choice options (*steadfast* and *bypass*) of through vehicles on Lane 1, some key conditions must be satisfied. First, from an aggregate perspective, through vehicles choosing the same option should have the same cost. Second, the cost should be an increasing function of the relevant traffic flows, reflecting the principle that higher traffic volumes

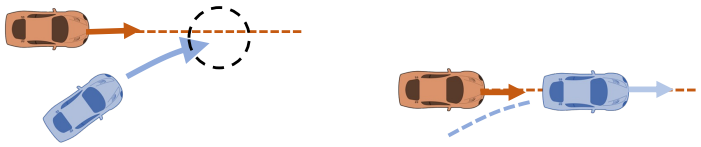

(a) Merging Behavior (b) Traversing Behavior

Figure 4: Two types of traffic interactions contribute to the costs of bypassing and steadfast behaviors: merging and traversing. Merging occurs when a vehicle attempts to enter another lane, often leading to delays due to conflicts with existing traffic. Traversing refers to the condition where many vehicles remain in the same congested lane. These two behaviors are key components of the cost structure in the weaving segment.

lead to greater travel difficulty and, consequently, higher costs. More specifically, a cost function can consist of two components: a traversing cost, which is proportional to the total flow on the chosen lane, and a merging cost, which is proportional to the product of the flows of merging parties.

The specific structure and parameter values of the cost model are determined through calibration and validation using data collected from simulations. The model is considered appropriate only when the calibration and validation results demonstrate satisfactory accuracy. For the sake of brevity, we omit the iterative design process and present only the final validated models. Let J_1^{s} denote the cost for through vehicles choosing the steadfast option, and J_1^{b} denote the cost for through vehicles choosing the bypassing option. We have the following costs J_1^{s} and J_1^{b}:

$$J_1^{\mathrm{s}}(\mathbf{x}) = C_1^{\mathrm{t}}\left(\alpha x_1^{\mathrm{s}} + \beta n_2^{\mathrm{exit}} + n_0^{\mathrm{enter}}\right) + C_1^{\mathrm{m}}\left(\omega x_1^{\mathrm{s}} n_2^{\mathrm{exit}} + x_1^{\mathrm{s}} n_0^{\mathrm{enter}}\right), \tag{9}$$

$$J_1^{\mathrm{b}}(\mathbf{x}) = C_2^{\mathrm{t}}\left(\gamma x_1^{\mathrm{b}} + n_2^{\mathrm{s}}\right) + C_2^{\mathrm{m}}\left(\rho x_1^{\mathrm{b}} n_2^{\mathrm{s}} + \delta x_1^{\mathrm{b}} n_2^{\mathrm{exit}}\right). \tag{10}$$

In the cost model, let C_i^{t} denote the unit traversing cost for Lane i, where $i \in \{1, 2\}$. After the strategic decisions of through vehicles, Lane 1 is shared by steadfast vehicles, exiting vehicles, and entering vehicles, while Lane 2 is occupied by bypassing vehicles and vehicles always traveling along Lane 2. The weight parameters α, β, γ are assumed to be positive, representing the relative impact on the cost compared to a standard traversing behavior. If a parameter value exceeds 1, it indicates a higher cost relative to normal traversing, possibly due to lower speeds or increased discomfort. Conversely, values less than 1 suggest a lower impact, while a value of 1 indicates a neutral, baseline cost. Similarly, let C_i^{m} represent the unit merging cost for Lane i, with ω, ρ, δ denoting the additional effort or discomfort associated with conflicting merging movements. A higher value of δ implies a more challenging merging process, reflecting the increased difficulty compared to standard merging behavior. Then let the cost coefficient vector be defined as $\mathbf{C} := (C_i^{\mathrm{t}}, C_i^{\mathrm{m}}, \alpha, \beta, \omega, \gamma, \rho, \delta \,|\, i \in \{1, 2\})$, which includes all the parameters that need be calibrated prior to the deployment on a new weaving ramp zone.

Remark 1 (Application Scenarios of Our Model). The proposed cost functions, which are proportional to flow rates, are particularly well-suited for modeling uncongested scenarios where traffic

flows smoothly. However, they may not fully capture the dynamics of congested conditions, such as queue formation, and thus are less applicable in oversaturated environments.

4.3 Existence and Uniqueness of HDVs' Wardrop Equilibrium

The aggregate lane choice equilibrium implies that each vehicle selects the option that minimizes its own cost, resulting in one of three outcomes: (1) all vehicles remain steadfast, (2) all vehicles bypass, or (3) a mixture of both behaviors if the costs J_1^{s} and J_1^{b} are equal. We now establish the existence and uniqueness of this equilibrium, showing how HDVs' equilibrium strategies vary across different exogenous conditions.

Theorem 1 (Existence and Uniqueness)**.** *For any given weaving ramp configuration* $G = (\mathbf{N}, \mathbf{C})$*, the equilibrium flow distribution vector* $\mathbf{x}$ *defined in Definition 1 always exists and is unique.*

The proof details are provided in Appendix 9.1. This proof establishes the existence and uniqueness of the HDV equilibrium, ensuring that a lane-choice equilibrium is guaranteed to exist for any real weaving ramp. With this result, our Wardrop-based lane choice model provides a well-defined baseline for subsequent analysis.

4.4 Parameter Calibration and Model Validation

In this section, we calibrate the parameters and validate the proposed Wardrop-based lane choice equilibrium model for HDVs. The data used for calibration are obtained from the microscopic traffic simulator SUMO (Krajzewicz et al., 2012). An overview of the simulated highway weaving ramp scenario is shown in Figure 3.

4.4.1 Parameter Calibration

To evaluate the performance of our model, we first calibrate the cost coefficient vector $\mathbf{C}$ using the optimization method detailed in (Mehr et al., 2021; Li et al., 2019). A broad range of scenarios is selected for data generation to ensure a comprehensive understanding of the model. Specifically, the simulations are conducted under a total flow rate of 1400 vehicles per hour. In the total flow rate, 600 vehicles per hour is allocated among the three neighboring vehicle types $f_2^{\mathrm{s}}, f_2^{\mathrm{exit}}, f_0^{\mathrm{enter}}$. The remaining flow rate of 800 vehicles per hour is set for f_1^{s} and f_1^{b}. This ensures sufficient interaction without triggering excessive congestion that could cause a deadlock in the simulation. We further fix the flow rate of one of the three vehicle types f_0^{enter}, f_2^{exit}, and f_2^{s} while varying the flow rates of the other two. This results in a total of 415 distinct data points. Each data point captures the equilibrium flow distribution vector $\mathbf{x} = (x_1^{\mathrm{s}}, x_1^{\mathrm{b}})$ for a simulation run with a given flow configuration $(n_0^{\mathrm{enter}}, n_2^{\mathrm{exit}}, n_2^{\mathrm{s}})$. To ensure that each simulation run reaches a steady state, we set each simulation duration to 20,000 timesteps, with the length of a single timestep as 1 second. All the vehicles have been successfully loaded into the simulation.

Solving the calibration optimization problem(Mehr et al., 2021; Li et al., 2019), which aims to find the best parameters that enable as many data points as possible to satisfy the condition in Definition 1, subject to the constraints on unit costs, we obtain:

$$C_1^{\mathrm{t}} = C_2^{\mathrm{t}} = 1, \tag{11}$$

$$C_1^{\mathrm{m}} = C_2^{\mathrm{m}} = 1. \tag{12}$$

We then obtain the calibrated cost coefficients as follows:

$$\alpha = 1.255, \quad \beta = 1.138, \quad \omega = 1.000, \tag{13}$$

$$\gamma = 2.384, \quad \delta = 3.094, \quad \rho = 1.000. \tag{14}$$

The above parameters reflect the relative impact of different vehicle interactions on the overall cost. Specifically, α and β are above 1 and $\omega = 1$, which suggests that the presence of steadfast vehicles in Lane 1 introduces additional discomfort or delay, possibly due to the increased conflicts and the need to brake and slow down. Further, lane-changing maneuvers of exiting vehicles disrupt the flow in Lane 1, increasing travel time or creating a need for additional adjustments by steadfast vehicles, while entering vehicles merge into Lane 1 without significantly disrupting the traffic flow, possibly due to the adequate space between the ramps leading to a neutral impact on steadfast vehicles. On lane 2, γ is significantly greater than 1, suggesting that the traversing cost for bypassing vehicles in Lane 2 is higher compared to the baseline traversing cost. This could be due to the increased discomfort of needing to maneuver around other vehicles, reflecting the high cost of making a bypass decision. And the higher value of δ suggests that conflicting merging movements significantly increase the cost by over three times than the standard merging cost. This reflects the increased difficulty and safety risks associated with such complex maneuvers, making it a significant factor in the decision-making process for through vehicles facing the weaving zone.

Remark 2 (Parameter values can reflect intrinsic characteristics of the weaving ramp). Although parameter magnitudes are determined through calibration, they are influenced by factors such as ramp geometry, speed limits, and other intrinsic features of the weaving zone. Hence, the calibrated values should be interpreted within the context of the specific scenario and may vary across different conditions. The effects of speed limits, vehicle gap, and driver aggressiveness on these parameters are analyzed in Appendix 9.2.

4.4.2 Model Validation

While validating our model, we selected a broad range of data to demonstrate its predictive accuracy and robustness. Specifically, we used 320 distinct data points, covering the range of $n_0^{\mathrm{enter}}, n_2^{\mathrm{exit}}, n_2^{\mathrm{s}} \in [0.2, 0.8]$, separate from the data points used for calibration, while ensuring the total demand across these three types of vehicles is fixed at 600 vehicles per hour, with no changes made to other parameters.

Fig. 5 presents the validation results, illustrating that the predictions of our lane choice model align closely with the observed simulation outcomes. Subfigures (a) and (c) indicate that, when the ratio of entering vehicles is fixed, increasing the proportion of exiting vehicles leads to more frequent interactions on Lane 1 and consequently more bypassing behavior by through vehicles, as they shift to Lane 2 to avoid congestion and reduced speeds. Subfigures (b) and (d) further illustrate that, when the normalized flow of through vehicles on Lane 2 is fixed, a higher entering ratio still results in more bypassing on Lane 1 than a higher exiting ratio. This finding indicates that entering vehicles exert a stronger influence on the bypassing behavior of through vehicles on Lane 1 than exiting vehicles. The phenomenon also corresponds to the high value of δ in the cost function, as exiting vehicles substantially increase the bypassing cost.

It is noteworthy that, despite the linear structure of our cost models, the lane choice model can still capture the nonlinear lane choice behavior observed in Fig. 5 due to the inherent nonlinearity of the inequalities governing the equilibrium conditions. As a result, our model demonstrates significant flexibility and minimal requirements for computation and calibration while satisfying accuracy.

5 Is the Selfish Behavior Socially Optimal?

Building on the Wardrop-based model introduced above, we further compare the user equilibrium (UE) and the socially optimal (SO) outcomes in this section. We first define the social cost J_{soc} as the total delay experienced by all vehicles within the weaving ramp, which is calculated as the sum of individual behavioral costs weighted by their corresponding flow magnitudes:

$$J_{\text{soc}}(\mathbf{x}) = x_1^{\text{s}} J_1^{\text{s}} + x_1^{\text{b}} J_1^{\text{b}} + n_2^{\text{s}} J_2^{\text{s}} + n_2^{\text{exit}} J_2^{\text{exit}} + n_0^{\text{enter}} J_0^{\text{enter}}, \tag{15}$$

where $J_1^{\text{s}}, J_1^{\text{b}}, J_2^{\text{s}}, J_2^{\text{exit}}, J_0^{\text{enter}}$ denote the cost functions corresponding to steadfast behavior on Lane 1, bypassing behavior on Lane 1, steadfast behavior on Lane 2, exiting from Lane 2, and entering from Lane 1, respectively. The detailed description of $J_2^{\text{s}}, J_2^{\text{exit}}$, and J_0^{enter} is provided in Section 6.1.

In Equation (15), we already know the cost function J_1^{s} and J_1^{b} from Equation (9) and (10). By following the formulation logic and structure form for these functions, we extend the cost functions for entering, exiting and through behaviors as follows:

$$J_2^{\text{s}}(\mathbf{x}) = C_2^{\text{t}}(\gamma x_1^{\text{b}} + n_2^{\text{s}}) + C_2^{\text{m}} x_1^{\text{b}} n_2^{\text{s}}, \tag{16}$$

$$J_2^{\text{exit}}(\mathbf{x}) = C_1^{\text{t}}(\alpha x_1^{\text{s}} + \beta n_2^{\text{exit}} + \omega n_0^{\text{enter}}) + C_1^{\text{m}}(x_1^{\text{s}} n_0^{\text{enter}} + x_1^{\text{s}} n_2^{\text{exit}}) + C_2^{\text{m}} \delta x_1^{\text{b}} n_2^{\text{exit}}, \tag{17}$$

$$J_0^{\text{enter}}(\mathbf{x}) = C_1^{\text{t}}(\alpha x_1^{\text{s}} + \beta n_2^{\text{exit}} + \omega n_0^{\text{enter}}) + C_1^{\text{m}}(x_1^{\text{s}} n_0^{\text{enter}} + x_1^{\text{s}} n_2^{\text{exit}}), \tag{18}$$

where C_i^{t} denotes the unit traversing cost on Lane $i \in [1, 2]$, C_i^{m} denotes the unit merging cost on Lane $i \in [1, 2]$, and the parameters $\alpha, \beta, \gamma, \omega, \delta$ capture the relative influence of different interactions on the overall cost. J_2^{s} is determined by congestion within the lane and the merging interactions caused by bypassing vehicles entering it. J_2^{exit} captures congestion arising from the traversing flow of steadfast, entering, and exiting vehicles, together with the merging difficulties as exiting vehicles

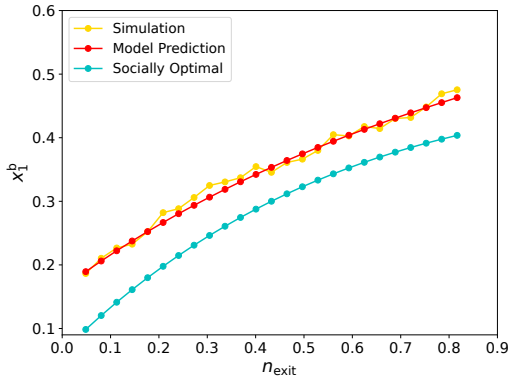

(a) Validation result with $n_{\text{enter}} = 0.1667$

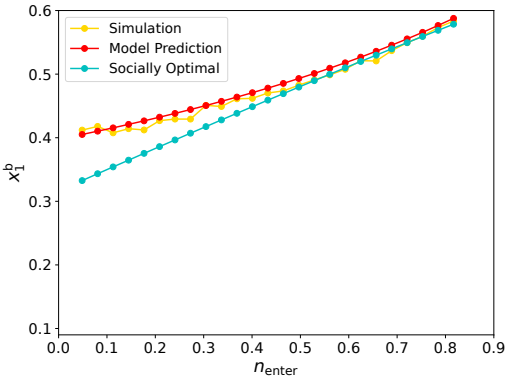

(b) Validation result with $n_2 = 0.1667$

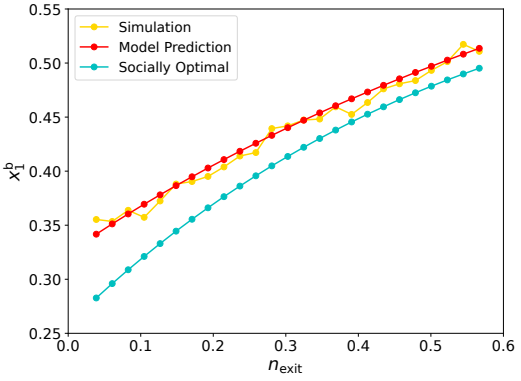

(c) Validation result with $n_{\text{enter}} = 0.4167$

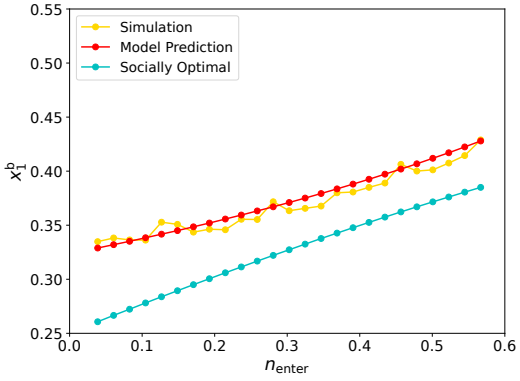

(d) Validation result with $n_2 = 0.4167$

Figure 5: Validation results demonstrate strong agreement between the proposed lane-choice model and observed simulation outcomes. Despite the underlying cost model is linear, the lane choice model successfully captures nonlinear behavior patterns due to the inherent nonlinearity of the equilibrium conditions. Moreover, the validation consistently reveals a gap between the equilibrium outcomes of our lane-choice model and the socially optimal benchmark across all tested configurations.

sequentially merge into Lanes 1 and 0. J_0^{enter} depends on congestion in Lane 1 and on the merging interactions between entering and exiting vehicles.

Equation (15) is then used to compute the socially optimal solution, illustrated as the "socially optimal" line in Figure 5. The numerical results show that HDVs' selfish decisions consistently deviate from the socially optimal outcomes. Subfigures (a) and (d) demonstrate a persistent gap between the Wardrop-based model predictions and the social optimum across all variations of exogenous normalized flows under fixed conditions $n_0^{\text{enter}} = 0.1667$ and $n_2^{\text{s}} = 0.4167$. Subfigures (b) and (c) reveal a similar pattern, when n_0^{enter} is small, the deviation between UE and SO is pronounced, but this gap gradually narrows as n_0^{enter} increases.

Thus, achieving socially optimal outcomes is inherently difficult in HDV-only environments. To enhance traffic efficiency and mitigate this inefficiency, we introduce two types of CAVs, which are

dedicated altruistic CAVs and **relaxed altruistic CAVs** as control mechanisms designed to improve overall system performance.

6 AVs as Dedicated Altruistic Decision Makers

The Wardrop-social optimality gap identified in the previous section highlights an opportunity for system-level intervention. To mitigate this inefficiency, we introduce dedicated altruistic CAVs, a class of AVs that follow externally mandated, system-oriented objectives. Such objectives can be communicated by a central authority through low-latency V2X links (Talebpour and Mahmassani, 2016). Unlike HDVs, whose behavior is driven by individual self-interest, dedicated altruistic CAVs' strategic behavior is governed by prescribed system-level goals. This unique characteristic makes them a promising mechanism for traffic management and optimization via strategic behavioral control. In this section, we develop a Stackelberg-Wardrop framework to capture the hierarchical interactions between CAVs and HDVs, and further investigate how system-level delays respond to varying CAV penetration rates through numerical experiments.

6.1 Updated Notations for Dedicated Altruistic CAVs

For simplicity of reference and analysis, we rewrite Equation (9), (10), (16), (17), and (18) as follows, where K_i^* ($i \in [0,1,2]$, $* \in \{\mathrm{s},\mathrm{b},\mathrm{exit},\mathrm{enter}\}$) aggregates all terms associated with variables x_1^{s} and x_1^{b}, B_i^* ($i \in [0,1,2]$, $* \in \{\mathrm{s},\mathrm{b},\mathrm{exit},\mathrm{enter}\}$) collects the remaining constant terms:

$$J_1^{\mathrm{s}}(\mathbf{x}) = K_1^{\mathrm{s}} x_1^{\mathrm{s}} + B_1^{\mathrm{s}}, \tag{19}$$

$$J_1^{\mathrm{b}}(\mathbf{x}) = K_1^{\mathrm{b}} x_1^{\mathrm{b}} + B_1^{\mathrm{b}}, \tag{20}$$

$$J_2^{\mathrm{s}}(\mathbf{x}) = K_2^{\mathrm{s}} x_1^{\mathrm{b}} + B_2^{\mathrm{s}}, \tag{21}$$

$$J_2^{\mathrm{exit}}(\mathbf{x}) = K_2^{\mathrm{exit}} x_1^{\mathrm{s}} + B_2^{\mathrm{exit}}, \tag{22}$$

$$J_0^{\mathrm{enter}}(\mathbf{x}) = K_0^{\mathrm{enter}} x_1^{\mathrm{s}} + B_0^{\mathrm{enter}}, \tag{23}$$

To explicitly characterize the control mechanism of dedicated altruistic CAVs, we further introduce q_{s} as the CAV steadfast proportion, with the remaining fraction $1 - q_{\mathrm{s}}$ corresponding to bypassing proportion. Here, q_{s} is controlled by the central command. When $q_{\mathrm{s}} = 1$, all CAVs remain steadfast; when $q_{\mathrm{s}} = 0$, all adopt bypassing. For intermediate values of $q_{\mathrm{s}} \in (0,1)$, a mixed strategy arises in which some CAVs remains steadfast while others bypass. Accordingly, the CAV flow proportions are given by:

$$x_{1,\mathrm{CAV}}^{\mathrm{s}} = p q_{\mathrm{s}}, \tag{24}$$

$$x_{1,\mathrm{CAV}}^{\mathrm{b}} = p(1 - q_{\mathrm{s}}), \tag{25}$$

Each behavioral cost J is a function of the CAV penetration rate p and the CAV steadfast proportion q_{s}. This formulation implies that the system-level delay can be directly influenced

through the strategic control of through CAVs on Lane 1. In particular, adjusting q_s for a given penetration rate p provides a lever for mitigating congestion and improving social efficiency.

6.2 The Stackelberg-Wardrop Framework

The interaction between CAVs and HDVs can be naturally represented by a **leader-follower structure**, reflecting their distinct behavioral characteristics. CAVs, with access to global system information through centralized controllers, can make informed decisions in advance, whereas HDVs rely solely on local observations of surrounding vehicles and respond based on observed behaviors.

To explicitly capture this leader–follower dynamic, a bilevel optimization framework is more appropriate than a single-level equilibrium model. Specifically, we adopt a Stackelberg game formulation (Başar and Olsder, 1999), in which the leader first commits to a strategy and the follower subsequently responds optimally given the leader's choice. This hierarchical structure aligns closely with the interaction logic between CAVs and HDVs in mixed-autonomy traffic systems. Within this framework, dedicated altruistic CAVs act as leaders, aiming to minimize the system's social cost (total delay), while selfish HDVs act as followers, individually seeking to minimize their own delays. The collective responses of HDVs are captured by the Wardrop equilibrium conditions previously introduced in Definition 1.

Thus, we propose a Stackelberg-Wardrop bilevel framework to model strategic lane choice behavior in mixed autonomy. In this framework, the upper-level is formulated as a Stackelberg game, where CAVs act as leaders and HDVs as followers. The lower-level follows the Wardrop equilibrium principle, capturing the adaptive responses of HDVs to the strategies selected by CAVs. The Stackelberg-Wardrop framework is defined as follows:

Definition 2 (Stackelberg–Wardrop Strategic Lane Choice Equilibrium)**.** For a given weaving ramp configuration $G = (\mathbf{N}, \mathbf{C})$ and CAV penetration rate $p \in [0, 1]$, let the Stackelberg–Wardrop flow vector be $\mathbf{x} := \big(x^{\mathrm{s}}_{1,\mathrm{CAV}} = pq_{\mathrm{s}},\, x^{\mathrm{b}}_{1,\mathrm{CAV}} = p(1-q_{\mathrm{s}}),\, x^{\mathrm{s}}_{1,\mathrm{HDV}},\, x^{\mathrm{b}}_{1,\mathrm{HDV}}\big)$. A flow vector $\mathbf{x}^*$ is a Stackelberg–Wardrop equilibrium if and only if the following bilevel conditions hold:

- *Upper level (CAV optimization).*

$$q_s^* \in \arg\min_{q_s \in [0,1]} J_{\mathrm{soc}}\big(\mathbf{x}^*\big). \tag{26}$$

- *Lower level (HDV lane-choice equilibrium).*

$$x^{\mathrm{s}}_{1,\mathrm{HDV}}\Big(J^{\mathrm{s}}_1(\mathbf{x}^*) - J^{\mathrm{b}}_1(\mathbf{x}^*)\Big) \le 0, \tag{27a}$$

$$x^{\mathrm{b}}_{1,\mathrm{HDV}}\Big(J^{\mathrm{b}}_1(\mathbf{x}^*) - J^{\mathrm{s}}_1(\mathbf{x}^*)\Big) \le 0,. \tag{27b}$$

This definition formalizes the Stackelberg–Wardrop equilibrium as a bilevel structure integrating centralized CAV control with decentralized HDV responses. The upper-level problem minimizes the social cost with respect to the CAV steadfast proportion q_{s}, while the objective implicitly depends on

HDV behavior determined by the lower-level lane choice equilibrium. This leads to a Mathematical Program with Equilibrium Constraints (MPEC), where the lower level is formulated as a Mixed Complementarity Problem (MCP) (Luo et al., 1996; Outrata et al., 2013). The interaction between HDVs and CAVs can be viewed as an iterative process: CAVs choose a tentative strategy allocation, HDVs respond by adjusting their lane choices, and the system iterates until neither side has an incentive to deviate.

Remark 3 (Residual Reformulation for Efficient Computation). To reduce the computational burden of repeatedly solving the lower-level equilibrium (27a) and (27b), we reformulate the complementarity conditions into continuous residual functions of the nonlinear complementarity problem (NCP), which allows the Sequential Quadratic Programming (SQP) algorithm to update upper-level variables without explicitly resolving the KKT system at each iteration. Specifically, the lane-choice equilibrium is enforced by requiring $h_1(x^{\mathrm{s}}_{1,\mathrm{HDV}}) = 0$ and $h_2(x^{\mathrm{b}}_{1,\mathrm{HDV}}) = 0$, where $h_1(x^{\mathrm{s}}_{1,\mathrm{HDV}}) = x^{\mathrm{s}}_{1,\mathrm{HDV}} \cdot \max(0, J^{\mathrm{s}}_1 - J^{\mathrm{b}}_1)$, and $h_2(x^{\mathrm{b}}_{1,\mathrm{HDV}}) = x^{\mathrm{b}}_{1,\mathrm{HDV}} \cdot \max(0, J^{\mathrm{b}}_1 - J^{\mathrm{s}}_1)$. Hence, by converting the bilevel problem into a tractable single-level nonlinear program, the proposed residual reformulation enables efficient computation without repeatedly solving the lower-level equilibrium problem.

6.3 Impact of Dedicated Altruistic CAVs

For the phase analysis, we denote two total steadfast proportion x^{s}_1 benchmarks as the **pure HDV equilibrium** at HDV-only environment ($p = 0$), denoted by Φ, and the **socially optimal equilibrium** for CAV-only environment ($p = 1$), denoted by Γ, respectively. Our focus is on configurations satisfying $\Phi < \Gamma$, which implies that under purely selfish behavior, fewer vehicles choose the steadfast strategy than in the socially optimal case. Furthermore, we define the **pure CAV equilibrium** at $p = 1$ as Ψ, we have $\Psi = \Gamma$ in this section, indicating that dedicated altruistic CAVs is fully altruism. The admissible set of configurations for the subsequent analysis is therefore refined as follows:

$$\mathcal{G} = \{G : 0 < \Phi < \Psi = \Gamma < 1\}, \tag{28}$$

To formalize behavioral transitions, we introduce two critical penetration thresholds: **Efficiency threshold** p_1, defined as the minimum penetration rate at which the social delay J_{soc} begins to decline. **Saturation threshold** p_2, defined as the penetration rate beyond which additional CAV deployment no longer produces further reductions in J_{soc}. For reference, we define the social delay in the absence of CAVs (i.e., $p = 0$) as the baseline social delay $J^{\mathrm{ref}}_{\mathrm{soc}}$.

Theorem 2 (Impact of Dedicated Altruistic CAVs on Social Delay)**.** *For any given weaving ramp configuration $G = (\mathbf{N}, \mathbf{C}) \in \mathcal{G}$, with CAV penetration rate p,*

- *The social delay remains invariant under dedicated altruistic CAVs, i.e., $J_{soc}(\mathbf{x}) = J^{ref}_{soc}$, if and only if $p \in \mathcal{A}_1$, where $\mathcal{A}_1 := [0, p_1]$,*

- *The social delay is decreased by dedicated altruistic CAVs, i.e.,* $J_{soc}(\mathbf{x}) < J_{soc}^{ref}$*, if and only if* $p \in \mathcal{A}_2$*, where* $\mathcal{A}_2 := (p_1, p_2]$*,*
- *The social delay is optimized by dedicated altruistic CAVs, i.e.,* $J_{soc}(\mathbf{x}) = J_{soc}^{opt}$*, if and only if* $p \in \mathcal{A}_3$*, where* $\mathcal{A}_3 := (p_2, 1]$*,*

where the two CAV penetration thresholds can be calculated as:

$$p_1 = \frac{K_1^b + B_1^b - B_1^s}{K_1^s + K_1^b}, \tag{29}$$

$$p_2 = \frac{2K_2 - K_3 + K_4}{2(K_1 + K_2)}. \tag{30}$$

The detailed proof is provided in Appendix 9.3. The proof sketch examines all possible cases as the CAV penetration rate p varies and analyzes the corresponding behaviors of both HDVs and CAVs. It shows that the social delay J_{soc} remains unchanged for $p \in [0, p_1]$, decreases for $p \in (p_1, p_2]$, and reaches its minimum for $p \in (p_2, 1]$. Furthermore, the theorem demonstrates that introducing dedicated altruistic CAVs effectively reduces the system delay and provides actionable guidance on the deployment scale and locations required to ensure system-level benefits.

Remark 4 (Flat Stage of Social Delay). When CAV penetration is low, the system experiences an initial plateau in the social cost J_{soc}. This occurs because selfish HDVs take advantage of the limited number of altruistic CAVs, benefiting individually while preventing immediate system-wide improvement.

6.4 Numerical Example for Stackelberg-Wardrop Framework

In this subsection, we present numerical examples to illustrate the impact of dedicated altruistic CAVs on both individual behavior and system-level performance as the CAV penetration rate p varies. The traffic demand is set to 60 entering vehicles on Lane 0, 30 exiting vehicles on Lane 1, 30 exiting vehicles on Lane 2, and 200 through vehicles on Lane 1 and Lane 2 per hour.

Figure 6a illustrates how the social cost J_{soc} varies with the CAV penetration rate p. When p is low, J_{soc} remains constant. It starts to decrease around $p \approx 0.6$, reaches reaches its optimal value near $p \approx 0.7$, and remains at this optimal level as p continues to increase. This pattern is consistent with the theoretical results established in Theorem 2.

Furthermore, we examine both system-level (social cost J_{soc}) in Figure 6a, individual-level (CAV steadfast proportion q_{s}) in Figure 6c, and individual CAV cost J_{CAV} in Figure 6b, where $J_{\text{CAV}} = p(J_1^{\text{s}} x_1^{\text{s}} + J_1^{\text{s}} x_1^{\text{b}}))$ impacts as the CAV penetration rate p increases. When p is low, q_{s} remains constant initially and then begins to adjust. During this stage ($0 \le p \le 0.6$), J_{soc} and J_{CAV} remain unchanged. This indicates that CAVs adjust their strategies to benefit the system while the overall social cost stays constant, mainly because HDVs exploit the altruistic contributions of CAVs, which aligns with Remark 4. As p further increases, such reduction comes at the cost of a significant increase in their individual cost, demonstrating their altruism toward society at their own expense.

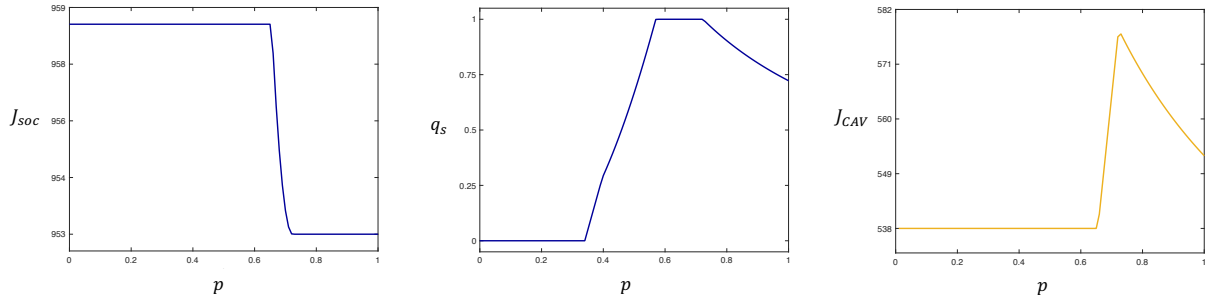

(a) Social cost under p (b) CAV strategy under p (c) Individual cost under p

Figure 6: These figures show the system-level and individual-level impact of CAV penetration rate p. Figure (a) shows how social cost J_{soc} changes during p increases. Figure (b) demonstrates how CAV steadfast proportion q_{s} changes when p increases. Figure (c) illustrates how each CAV's cost changes when p increases.

Finally, once J_{soc} reaches its minimum, J_{CAV} begins to decline, suggesting that dedicated altruistic CAVs can eventually benefit themselves once their market share becomes sufficiently large.

7 AVs as Relaxed Altruistic Decision Makers

In practice, CAVs and HDVs rarely adhere to strictly homogeneous behavioral rules. Instead, they exhibit heterogeneous characteristics in decision-making and interactions. A more realistic framework therefore considers relaxed altruistic CAVs, whose objectives reflect a weighted combination of self-interest and social welfare. For HDVs, we characterize their behavioral diversity using the Social Value Orientation (SVO) framework (Van Lange, 1999), which encompasses altruistic, selfish, competitive, and other extreme orientations. In this section, we analyze the performance of relaxed altruistic CAVs under varying penetration rates p within heterogeneous environments, compare their outcomes with those of dedicated altruistic CAVs, and discuss potential mechanisms to incentivize altruistic behavior to enhance overall system efficiency and CAV–HDV interactions.

7.1 Updated Notations for Relaxed Altruistic CAVs

As we extend the analysis from dedicated altruistic CAVs and selfish HDVs to a more heterogeneous setting, both CAVs and HDVs are represented by vehicles types with different SVO levels. Accordingly, we denote j as the vehicle type, and update the steadfast and bypassing flow ratios as $x^{\text{s}}_{1,j}$ and $x^{\text{b}}_{1,j}$, respectively, where each type j is associated with a specific SVO level θ_j.

Furthermore, we define the cost functions of SVO-level vehicles as a weighted combination of individual travel delay and marginal social cost, capturing their trade-off between self-interest and social welfare. The marginal social cost is defined as the additional total system delay generated by one more vehicle adopting a given strategy (Beckmann et al., 1956), which we mathematically represent as the partial derivative of the social cost with respect to the corresponding flow. Let $\tilde{J}^{\text{s}}_{1,j}$ and $\tilde{J}^{\text{b}}_{1,j}$ denote the cost function for steadfast and bypassing vehicles, respectively. To capture

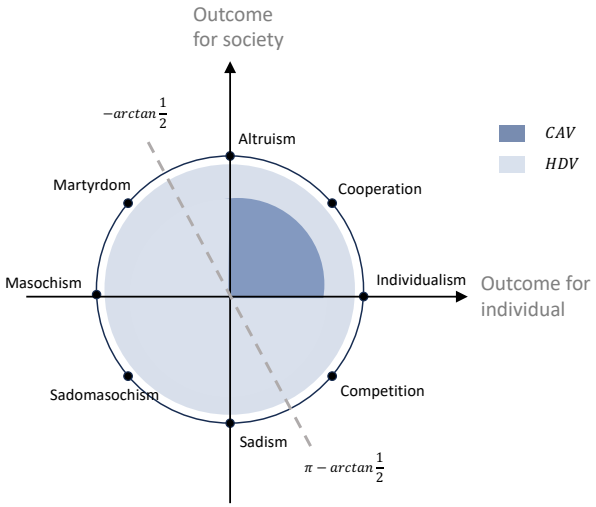

Figure 7: This figure illustrates the SVO circle (Liebrand et al., 1986), where each vehicle type j is characterized by an angle θ_j representing its orientation toward individual versus collective outcomes. The x-axis denotes concern for individual outcomes, and the y-axis denotes concern for societal outcomes. Positive values indicate prosocial orientations, negative values reflect competitive or antagonistic tendencies, and zero represents neutrality. In our setting, we focus on the subset of orientations satisfying $\cos\theta_j + \sin\theta_j > 0$, which corresponds to vehicle types whose combined valuation of individual and social outcomes is positive.

the heterogeneity in social preferences, we introduce the SVO parameter θ_j, illustrated in Figure 7. Specifically, $\theta_j = 0$ corresponds to purely selfish behavior, $\theta_j = \frac{\pi}{2}$ represents fully altruistic behavior, and $\theta_j = (0, \frac{\pi}{2})$ indicates partially altruistic behaviors. Extreme altruism is described by $\theta_j \in (\frac{\pi}{2}, \pi]$. Negative values capture non-cooperative orientations: $\theta_j \in (-\frac{\pi}{2}, 0)$ denotes competitive behavior, and $\theta_j \in (-\pi, -\frac{\pi}{2})$ corresponds to extreme sadomasochism tendencies, which may be interpreted as pathological driving behaviors. In this formulation, $sin(\theta_j)$ captures the vehicle's orientation toward social welfare, while $cos(\theta_j)$ reflects the weight placed on individual outcomes. Thus, we have the cost function for steadfast and bypassing vehicles $\tilde{J}^{\mathrm{s}}_{1,j}$ and $\tilde{J}^{\mathrm{b}}_{1,j}$ as:

$$\tilde{J}^{\mathrm{s}}_{1,j}(\mathbf{x}) = cos(\theta_j) J^{\mathrm{s}}_1(\mathbf{x}) + sin(\theta_j) \frac{\partial J_{\mathrm{soc}}(\mathbf{x})}{\partial x^{\mathrm{s}}_{1,j}}, \tag{31}$$

$$\tilde{J}^{\mathrm{b}}_{1,j}(\mathbf{x}) = cos(\theta_j) J^{\mathrm{b}}_1(\mathbf{x}) + sin(\theta_j) \frac{\partial J_{\mathrm{soc}}(\mathbf{x})}{\partial x^{\mathrm{b}}_{1,j}}, \tag{32}$$

Remark 5 (CAV–HDV Behavioral Differentiation). HDVs and CAVs are distinguished by their respective ranges of the SVO parameter θ_j. For relaxed altruistic CAVs, θ_j is constrained within $0 \leq \theta_j \leq \frac{\pi}{2}$, reflecting their controllable and cooperative nature. In contrast, HDVs are assigned $-\pi \leq \theta_j \leq \pi$, representing the wider behavioral diversity and unpredictability of human drivers.

7.2 Heterogeneous Wardrop Framework

In the mixed-autonomy setting, both CAVs and HDVs adopt the cost functions defined in Equations (31) and (32), respectively. All vehicle types are assumed to satisfy Wardrop's principle, leading to the following heterogeneous Wardrop framework:

Definition 3 (Heterogeneous Wardrop Lane Choice Equilibrium)**.** For a given weaving-ramp configuration $G = (\mathbf{N}, \mathbf{C})$, a flow distribution vector $\mathbf{x}$ is in equilibrium if and only if

$$x^{\mathrm{s}}_{1,j}(\tilde{J}^{\mathrm{s}}_{1,j}(\mathbf{x}) - \tilde{J}^{\mathrm{b}}_{1,j}(\mathbf{x})) \leq 0, \tag{33a}$$

$$x^{\mathrm{b}}_{1,j}(\tilde{J}^{\mathrm{b}}_{1,j}(\mathbf{x}) - \tilde{J}^{\mathrm{s}}_{1,j}(\mathbf{x})) \leq 0, \tag{33b}$$

for all vehicle classes $j = 1, 2, \ldots, J$.

7.3 Impact of Relaxed Altruistic CAVs

There are H types of HDVs, indexed by $h \in \mathcal{H}$ with within-HDV shares w_h^{HDV}, where $h = 1, 2, \cdots, H$. Similarly, there are C types of CAVs, indexed by $c \in \mathcal{C}$ with within-CAV shares w_c^{CAV}, where $c = 1, 2, \cdots, C$. All vehicle types belong to $j = 1, \cdots, J$. By definition, $\sum_{h\in\mathcal{H}} w_h^{\mathrm{HDV}} = 1$ and $\sum_{c\in\mathcal{C}} w_c^{\mathrm{CAV}} = 1$. Given a CAV penetration rate $p \in [0, 1]$, the overall population shares are given by:

$$w_{j=h}(p) = (1-p)w_h^{\mathrm{HDV}}, \qquad w_{j=c}(p) = pw_c^{\mathrm{CAV}}. \tag{34}$$

where naturally $\sum_{h=1}^{H} w_{j=h}(p) + \sum_{c=1}^{C} w_{j=c}(p) = 1$.

Theorem 3 (Impact of Relaxed Altruistic CAVs on Social Delay)**.** *Consider a weaving-ramp configuration $G = (N, \mathcal{C})$ with CAV penetration rate $p \in [0, 1]$ and vehicle types $j = 1, \cdots, J$. Assume that, for every vehicle type j $\cos(\theta_j)+2\sin(\theta_j) > 0$, and that the thresholds $\{\chi_j\}_{j=1}^{J} = \frac{B^b_{1,j}+K^b_{1,j}-B^s_{1,j}}{K^s_{1,j}+K^b_{1,j}}$ are pairwise distinct. For each admissible index k, define:*

$$W_k(p) := \sum_{j:\chi_j>\chi_k} w_j(p), \qquad I_k := \{p \in [0, 1] : 0 < \chi_k - W_k(p) < w_k(p)\}. \tag{35}$$

Then the following statements hold:

- *For any $p \in [0, 1]$, at most one vehicle type can be mixed.*
- *$p \in I_k$ if and only if type k is the unique mixed type, all types with $\chi_j > \chi_k$ are fully steadfast, and all types with $\chi_j < \chi_k$ are fully bypass.*
- *On I_k, the equilibrium steadfast proportion $x_1^{s*} = \chi_k$, since J_{soc} depends only on x_1^s, J_{soc} is constant on I_k.*

- *The boundaries of the constant interval I_k are determined by the two linear equations:*

$$W_k(p) = \chi_k, \quad W_k(p) + w_k(p) = \chi_k. \tag{36}$$

The onset and termination of the plateau associated with type k are the penetration rates at which type k first becomes active and then becomes fully steadfast or bypass.

- *A specific penetration range $\mathcal{P} \subseteq [0,1]$ is free of constant social-delay intervals if and only if $\mathcal{P} \cap I_k = \varnothing$, $\forall k = 1, \cdots, J$.*

The detailed proof is provided in Section 9.4. The proof first orders vehicle types by their thresholds χ_j, then characterizes the unique mixed type on each interval I_k, and finally shows that $x_1^{s*} = \chi_k$ on I_k, implying that J_{soc} remains constant on each such interval.

The above results provide a structural characterization of penetration ranges that induce constant social delay. In particular, each interval I_k corresponds to a plateau induced by vehicle type k, and the union $\mathcal{I} := \bigcup_{k=1}^{J} I_k$ captures all such undesirable regimes. Therefore, this characterization enables the design of target penetration ranges $\mathcal{P}$ that avoid these constant-delay regions, i.e., $\mathcal{P} \cap \mathcal{I} = \varnothing$, which ensures that improvements in social cost can be achieved as the penetration rate varies within $\mathcal{P}$.

This result highlights that, under heterogeneous behavioral responses, increasing CAV penetration rate p only does not necessarily lead to monotonic improvements in system performance. Instead, the social cost J_{soc} exhibits a piecewise-constant structure, remaining unchanged within each interval I_k and varying only when the active vehicle type switches. Each plateau is associated with a specific vehicle type k, indicating that the emergence of inefficiency is intrinsically linked to the distribution of behavioral preferences across vehicles. Consequently, system performance depends not only on the penetration rate p, but also on the composition of heterogeneous CAV types. Importantly, this structural characterization enables the identification and avoidance of penetration regimes that induce constant social delay, thereby providing a principled approach for designing CAV deployment strategies that achieve meaningful improvements in social cost.

7.4 Numerical Example for Heterogeneous Wardrop Framework

In this subsection, we do numerical examples to show comparisons impacts between relaxed altruistic CAVs and dedicated altruistic CAVs, and demonstrate insights in Theorem 3. In this simulation, we conduct 30 entering vehicles on Lane 0, 10 exiting vehicles on Lane 1, 10 exiting vehicles on Lane 2, and 50 through vehicles on Lane 1 and Lane 2 per hour.

For Figure 8a, we compare two settings: (i) a homogeneous scenario with a single type of relaxed altruistic CAVs and a single type of selfish HDVs, and (ii) a heterogeneous scenario involving multiple types of relaxed altruistic CAVs and HDVs. In both cases, the social cost initially remains stable, then decreases, and ultimately converges toward the optimal level, consistent with the trend described in Theorem 3. Notably, in the heterogeneous scenario, the onset of social cost reduction

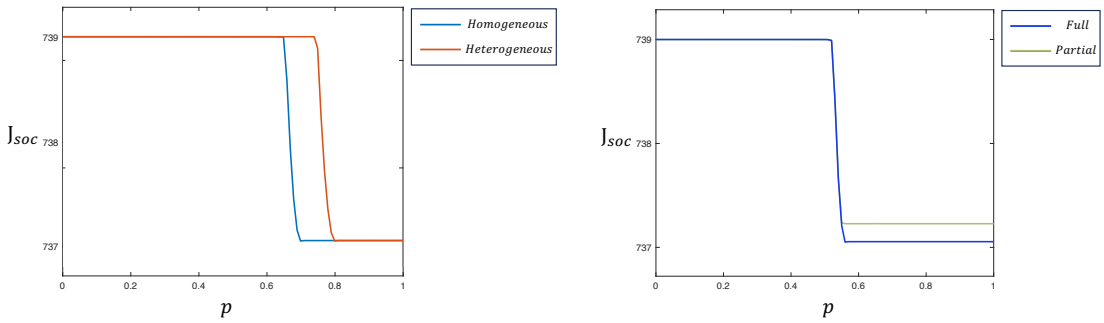

(a) Heterogeneous vs. Homogeneous Phase (b) Full vs. Partial Altruism Phase

Figure 8: Figure (a) presents the social cost phase comparison between homogeneous and heterogeneous scenarios. The homogeneous scenario involves single type of dedicated altruism CAVs, whereas the heterogeneous scenario consists of multiple types of relaxed altruistic CAVs. Figure (b) provides a comparison between relaxed altruistic CAVs and dedicated altruistic CAVs in the homogeneous scenario.

is delayed, beginning near $p = 0.75$, and stabilizing around $p = 0.8$, compared to the homogeneous case, where the transition occurs earlier, between $p = 0.65$ and $p = 0.7$. This delay highlights how the diversity of vehicle types and behavioral heterogeneity can influence the rate and extent of system improvement as CAV penetration increases.

For Figure 8b, we further examine the difference between dedicated altruistic CAVs and relaxed altruistic CAVs in homogeneous settings. While relaxed altruistic CAVs contribute to reducing the social cost J_{soc}, their impact plateaus at high penetration levels, leading to a noticeable gap relative to dedicated altruistic CAVs. This finding suggests that partial altruism, though beneficial, cannot fully replicate the societal gains achieved under complete altruism. From a policy perspective, this implies that moderate levels of altruistic design or incentive mechanisms may improve system performance without requiring fully altruistic vehicle control, but achieving the social optimum still necessitates stronger coordination or regulatory intervention.

Furthermore, we design four types of CAVs with $\theta_{1,1} = \frac{1}{5}\pi$, $\theta_{1,2} = \frac{1}{4}\pi$, $\theta_{1,3} = \frac{1}{3}\pi$, and $\theta_{1,4} = \frac{1}{2}\pi$, with corresponding within-CAV shares $w_1^{\text{HDV}} = 0.1$, $w_2^{\text{HDV}} = 0.2$, $w_3^{\text{HDV}} = 0.3$, and $w_4^{\text{HDV}} = 0.4$. The evolution of the social cost J_{soc} and the steadfast proportions of each vehicle type are illustrated in Figure 9. The results reveal a clear multi-stage structure in the evolution of J_{soc} as the penetration rate p increases. In particular, J_{soc} remains constant within each interval and decreases only at specific transition points. This piecewise-constant behavior directly corresponds to the interval structure characterized in Theorem 3, where each interior interval I_k is associated with a unique active mixed vehicle type.

From Figure 9b, we observe that as p increases, different vehicle types sequentially become the active mixed type in the equilibrium. Within each interval, only one vehicle type exhibits a mixed strategy, while all other types are either fully steadfast or fully bypass. As predicted by Theorem 3, this implies that the aggregate steadfast proportion x_1^{s} remains fixed at the corresponding threshold χ_k, leading to a constant value of J_{soc} in Figure 9(a). At the boundary of each interval, a regime-

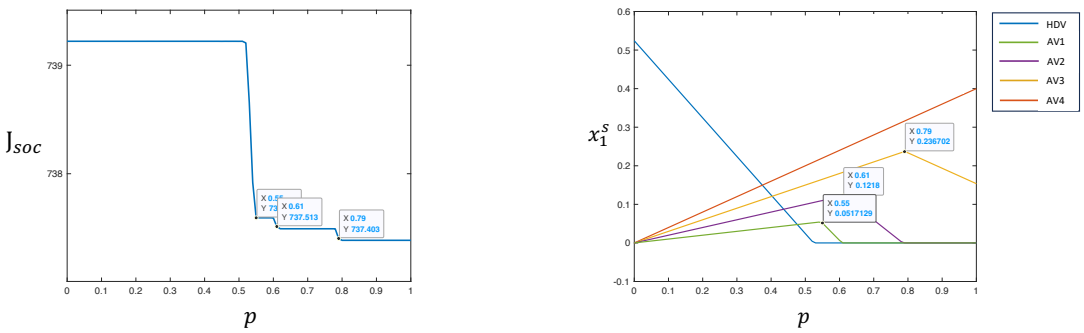

(a) Social cost under p

(b) Vehicle strategies under p

Figure 9: Figure (a) presents the change of the social cost J_{soc} as the CAV penetration rate p varies in the heterogeneous mixed-autonomy setting. Figure (b) shows the corresponding change of each vehicle type j's steadfast proportion x_1^{s}. The results illustrate that the multi-stage evolution of J_{soc} corresponds to changes in the active mixed vehicle type k, which partitions the parameter range into several equilibrium regimes.

switching event occurs: the previously active mixed type becomes pure, and a new vehicle type takes over as the active mixed type. This transition causes a discrete shift in the equilibrium steadfast proportion x_1^{s}, which in turn produces a stepwise change in the social cost. As a result, the overall evolution of J_{soc} follows a staircase-like pattern, where each plateau corresponds to a specific behavioral type. These results highlight that the multi-stage evolution of system performance is driven by the sequential activation of heterogeneous vehicle types. Rather than improving continuously with p, the system exhibits periods of stagnation (plateaus) followed by abrupt improvements at regime-switching points. This mechanism underscores the critical role of behavioral heterogeneity in shaping both the structure and timing of efficiency gains in mixed-autonomy traffic systems.

Figures 8 and 9 jointly illustrate how behavioral heterogeneity shapes the evolution of the social cost as the CAV penetration rate increases. While both homogeneous and heterogeneous settings eventually achieve reductions in social cost, the heterogeneous case exhibits a delayed onset of improvement and a distinct multi-stage transition pattern. These results are consistent with Theorem 3, where the penetration range is partitioned into intervals I_k associated with different active vehicle types. As the penetration rate increases, regime switching between these intervals leads to stepwise changes in the equilibrium and the social cost. Overall, the results demonstrate that heterogeneous behavioral preferences not only affect the magnitude of efficiency gains but also induce a multi-stage, staircase-like evolution of system performance.

8 Conclusions

This study develops a unified modeling framework to investigate how altruistic and strategic behaviors of CAVs affect lane choice and congestion at highway weaving ramps. Starting from a Wardrop formulation for HDVs, we construct a bilevel Stackelberg–Wardrop model capturing

strategic CAV leadership and HDV equilibrium responses, and further extend it to a heterogeneous Wardrop framework incorporating SVO-based behavioral diversity.

Analytical and numerical results consistently reveal that altruistic CAVs can effectively reduce social delay, but the improvement is not monotonic. Instead, the system exhibits a multi-stage, piecewise-constant evolution, where the social cost remains unchanged within certain penetration intervals and decreases only at regime-switching points, which shows that each plateau corresponds to a specific active vehicle type. Behavioral heterogeneity reshapes these intervals, delaying the onset of improvements and altering the transition path, but does not negate the overall benefits of altruistic behavior.

Future extensions will incorporate dynamic and stochastic environments to model time-varying demand, adaptive learning, and behavioral uncertainty, enabling analysis of temporal effects in realistic traffic systems. We also plan to generalize the framework to network-level applications such as multi-ramp corridors and interconnected mixed-autonomy networks. Ultimately, this research provides a foundation for designing incentive and regulatory mechanisms that harness strategic altruism to achieve equitable and efficient future mobility systems.

9 Appendix

9.1 Proof for Theorem 1

Proof. To prove Theorem 1, we first write the cost functions for through vehicles as follows:

$$J_1^{\mathrm{s}}(\mathbf{x}) = C_1^{\mathrm{t}}\left(\alpha x_1^{\mathrm{s}} + \beta n_{\mathrm{exit}} + n_{\mathrm{enter}}\right) + C_1^{\mathrm{m}}\left(\omega x_1^{\mathrm{s}} n_2^{\mathrm{exit}} + x_1^{\mathrm{s}} n_0^{\mathrm{enter}}\right), \tag{37}$$

$$J_1^{\mathrm{b}}(\mathbf{x}) = C_2^{\mathrm{t}}\left(\gamma(1-x_1^{\mathrm{s}}) + n_2^{\mathrm{s}}\right) + C_2^{\mathrm{m}}\left(\rho(1-x_1^{\mathrm{s}}) n_2^{\mathrm{s}} + \delta(1-x_1^{\mathrm{s}}) n_2^{\mathrm{exit}}\right), \tag{38}$$

Next, we analyze the behavior of the cost functions with respect to x_1^{s}:

- $\frac{\partial J_1^{\mathrm{s}}}{\partial x_1^{\mathrm{s}}} = C_1^{\mathrm{t}}\alpha + C_1^{\mathrm{m}}(\omega n_2^{\mathrm{exit}} + n_0^{\mathrm{enter}})$, which is a positive constant, making $J_1^{\mathrm{s}}(\mathbf{x})$ an increasing affine function of x_1^{s}.
- $\frac{\partial J_1^{\mathrm{b}}}{\partial x_1^{\mathrm{s}}} = -C_2^{\mathrm{t}}\gamma - C_2^{\mathrm{m}}(\rho n_2^{\mathrm{s}} + \delta n_2^{\mathrm{exit}})$, which is a negative constant, making $J_1^{\mathrm{b}}(\mathbf{x})$ a decreasing affine function of x_1^{s}.

The above properties ensure that the cost functions can intersect at most once, which directly implies that the equilibrium is unique. Let us consider three scenarios based on the relative magnitudes of $J_1^{\mathrm{s}}(\mathbf{x})$ and $J_1^{\mathrm{b}}(\mathbf{x})$:

- Case (a): For all $x_1^{\mathrm{s}} \in [0,1]$, $J_1^{\mathrm{s}}(\mathbf{x}) > J_1^{\mathrm{b}}(\mathbf{x})$. This implies that all vehicles will choose to bypass, resulting in $x_1^{\mathrm{s}} = 0$ and $x_1^{\mathrm{b}} = 1$.
- Case (b): $J_1^{\mathrm{s}}(\mathbf{x})$ and $J_1^{\mathrm{b}}(\mathbf{x})$ intersect at a unique point $\bar{x}_1^{\mathrm{b}} \in (0,1)$. This intersection defines the unique equilibrium distribution, where $x_1^{\mathrm{s}} = x_1^{\mathrm{s}*}$ and $x_1^{\mathrm{b}} = 1 - x_1^{\mathrm{s}*}$.

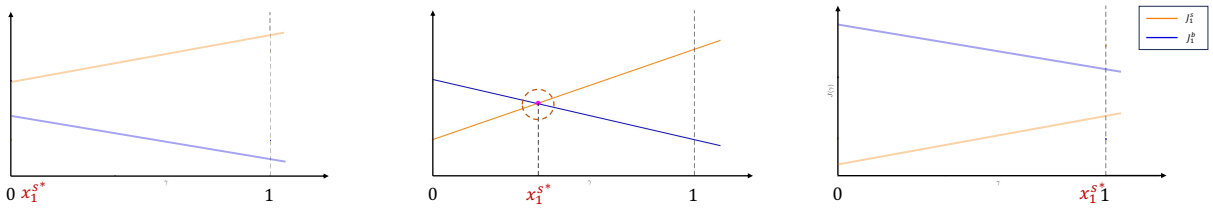

(a) Case(a) (b) Case(b) (c) Case(c)

Figure 10: These figures show three equilibrium cases for HDVs. For Case(a), The bypassing delay cost is consistently higher than the steadfast delay cost across all flow ratios, leading to the equilibrium flow rates $x_1^{\mathrm{s}} = 0$. For Case(b), the bypassing and steadfast delay cost functions intersect, resulting in a mixed equilibrium where both strategies are used: $x_1^{\mathrm{b}} > 0, x_1^{\mathrm{s}} > 0$. For Case(c), The bypassing delay cost is strictly lower than the steadfast delay cost for all flow ratios, yielding an equilibrium of $x_1^{\mathrm{s}} = 1$.

- Case (c): For all $x_1^{\mathrm{s}} \in [0, 1]$, $J_1^{\mathrm{s}}(\mathbf{x}) < J_1^{\mathrm{b}}(\mathbf{x})$. In this scenario, all vehicles will remain steadfast, resulting in $x_1^{\mathrm{s}} = 1$ and $x_1^{\mathrm{b}} = 0$.

Thus, in all cases, the equilibrium exists and is unique. This concludes the proof. □

9.2 The Baseline Model Analysis

Table 1: Mean Prediction Error Rates (MPER) of the cost function calibrated by the data points in 4.4 in different experimental scenarios. The formula for calculating the MPER is: MPER $= \frac{\sum_{i=1}^{n} \left| \frac{x_{1,\mathrm{S},i}^{\mathrm{s}} - x_{1,\mathrm{M},i}^{\mathrm{s}}}{x_{1,\mathrm{S},i}^{\mathrm{s}}} \right|}{n} \times 100\%$, in which n is the length of test set; $x_{1,\mathrm{S},i}^{\mathrm{s}}$ is the i^{th} simulation-generated x_1^{s} in the test set; $x_{1,\mathrm{M},i}^{\mathrm{s}}$ is the i^{th} x_1^{s} predicted by our model. $\mathrm{MPER}_{n_i}^{0.1667}$ represents the experiments with its constant flow $n_i = 0.1667$ for $i \in \{0, 2\}$, while $\mathrm{MPER}_{n_i}^{0.4167}$ represents the experiments with its constant flow $n_i = 0.4167$ for $i \in \{0, 2\}$

Expt.	$\mathrm{MPER}_{n_0^{\mathrm{enter}}}^{0.1667}$	$\mathrm{MPER}_{n_2^{\mathrm{s}}}^{0.1667}$	$\mathrm{MPER}_{n_0^{\mathrm{enter}}}^{0.4167}$	$\mathrm{MPER}_{n_2^{\mathrm{s}}}^{0.4167}$
4.4	1.15%	1.55%	1.00%	1.05%
1-1	5.51%	3.52%	2.41%	4.79%
1-2	5.89%	11.00%	8.36%	1.85%
2-1	2.54%	3.07%	3.18%	4.30%
2-2	1.79%	2.23%	2.74%	1.18%
3-1	1.13%	1.26%	1.21%	0.72%
3-2	1.15%	1.36%	1.01%	0.87%
3-3	1.04%	1.36%	1.10%	0.96%

To test the robustness of our model, we conduct the following three sets of univariate experiments:

1. Adjust the velocity limits of through vehicles on lane 2 from 20 m/s to 12.5 m/s (Expt. 1-1) and the velocity limits of exiting vehicles from 20 m/s to 13.9 m/s (Expt. 1-2).

2. Adjust the minimum gap (the minimum distance a vehicle can maintain from the vehicle ahead) of through vehicles on lane 2 (Expt. 2-1) and entering vehicles (Expt. 2-2) from 2m to 10m.

3. Increase the vehicle aggressiveness level of through vehicles on lane 2 (Expt. 3-1), exiting vehicles (Expt. 3-2) and entering vehicles (Expt. 3-3)

We input the data points collected from the experiments into the cost function calibrated by the data points in 4.4. For each test, we set either n_0^{enter} or n_2^{s} as constant, with values of $n_0^{\text{enter}}, n_2^{\text{s}} \in \{0.1667, 0.4167\}$, following the method used in the model validation section to select data points. From each test, we obtain 100 data points: 50 data points are collected when n_0^{enter} is constant (25 data points for $n_0^{\text{enter}} = 0.1667$ and 25 data points for $n_0^{\text{enter}} = 0.4167$), and the remaining 50 data points are collected while n_2^{s} is constant. As the table 1 shows, all of the mean prediction error rates in different experimental scenarios are no larger than 11%, which shows that the model is robust.

To explore the practical significance implied by each parameter in the model, thereby enabling informed adjustments under different environmental configurations to maintain accurate model performance, we recalibrate our model using the configuration adjusted in the experiments. The results are shown in Table 2 and Table 3.

Table 2: Model parameters under different configurations.

Expt.	α	β	ω	γ	ρ	δ
4.4	1.255	1.138	1.000	2.384	1.000	3.094
1-1	1.323	2.618	1.000	2.323	1.000	6.240
1-2	1.178	2.002	1.000	2.116	1.000	8.266
2-1	1.000	1.000	1.030	2.323	1.123	2.459
2-2	1.236	1.000	1.000	2.204	1.044	2.726
3-1	1.302	1.056	1.000	2.436	1.000	2.958
3-2	1.324	1.000	1.000	2.475	1.000	2.835
3-3	1.294	1.000	1.076	2.417	1.000	2.985

The results of experiments show that parameters ω and ρ have very strong robustness since they gained a 0% fluctuating rate in most of the experiments, while they only obtained a minimal fluctuating rate in some specific experiments. Parameters α and γ also performed robustly, keeping the absolute value of the fluctuating rate below 25% in all experiments. Parameters β and δ acted robustly in experiments 2 and 3, as all the absolute values of the fluctuating rates are below 25% in both experiments. Meanwhile, both values gained a high fluctuating rate when the velocity of vehicles in the scenario changed. Given that the results show the changing trends of different parameters under various factors, the model parameters can be adjusted accordingly in new experimental environments to achieve more accurate prediction performance.

In conclusion, we validated the accuracy of our model and further assessed its robustness across different experimental scenarios. By recalibrating the model under various experimental conditions, we identified the variation patterns of model parameters across scenarios with different configura-

Table 3: The fluctuating rate (FR) between model parameters calibrated under different configurations and the configuration we used in 4.4 . The formula for calculating the fluctuating rate is: $\mathrm{FR} = \frac{x_{\mathrm{exp}} - x_{\mathrm{ori}}}{x_{\mathrm{ori}}} \times 100\%$. If $\mathrm{FR} > 0$, the parameters obtained from the experiments are larger than the corresponding parameters we calibrated in 4.4. Otherwise, if $\mathrm{FR} < 0$, the parameters obtained from the experiments are smaller than the corresponding parameters from 4.4. The bold data represent parameters that have significant differences ($|\mathrm{FR}| > 25\%$) compared to the parameters from 4.4.

Expt.	α	β	ω	γ	ρ	δ
1-1	5.42%	**130.05%**	0.00%	-2.56%	0.00%	**101.68%**
1-2	-6.13%	**75.92%**	0.00%	-11.24%	0.00%	**167.16%**
2-1	-20.32%	-12.13%	3.00%	-2.56%	12.30%	-20.52%
2-2	-1.51%	-12.13%	0.00%	-7.55%	4.40%	-11.89%
3-1	3.75%	-7.21%	0.00%	2.18%	0.00%	-4.40%
3-2	5.50%	-12.13%	0.00%	3.82%	0.00%	-8.37%
3-3	3.11%	-12.13%	7.60%	1.38%	0.00%	-3.52%

tions. These findings enable the model to achieve accurate prediction performance by adjusting the corresponding parameters when applied to unprecedented weaving ramp scenarios not included in our training data. Therefore, our model demonstrates strong practicality when applied to previously unseen scenarios.

9.3 Proof for Theorem 2

Proof. In this problem, the decision variable is steadfast proportion $q_{\mathrm{s}} \in [0, 1]$. The CAV penetration rate $p \in [0, 1]$ is given. From Equation (6) and (24), the range of CAV steadfast proportion $x^{\mathrm{s}}_{1,\mathrm{CAV}} \in [0, p]$, and the range of HDV steadfast proportion $x^{\mathrm{s}}_{1,\mathrm{HDV}} \in [0, 1-p]$.

In Appendix 9.1, the existence and uniqueness of HDV equilibrium is proved. In Equation (27), the lower level is the HDV equilibrium, thus the lower level satisfies the uniqueness and existence. Then we prove the existence and uniqueness of upper level CAV optimization:

In Equation (26), q^*_{s} is the point that can let J_{soc} reaches the minimum value. Thus, in order to prove the existence and uniqueness of q^*_{s}, the existence and uniqueness of minimum J_{soc} needs to be proved. The social cost J_{soc} can be expressed as a function of the total steadfast proportion x^{s}_1:

$$\begin{aligned} J_{\mathrm{soc}} = {} & (K^{\mathrm{s}}_1 + K^{\mathrm{b}}_1)(x^{\mathrm{s}}_1)^2 + (-2K^{\mathrm{b}}_1 + n^{\mathrm{exit}}_2 K^{\mathrm{exit}}_2 + n^{\mathrm{enter}}_0 K^{\mathrm{enter}}_0 + B^{\mathrm{s}}_1 - n^{\mathrm{s}}_2 K^{\mathrm{s}}_2 - B^{\mathrm{b}}_1) x^{\mathrm{s}}_1 \\ & + K^{\mathrm{b}}_1 + n^{\mathrm{s}}_2 K^{\mathrm{s}}_2 + B^{\mathrm{b}}_1 + B_{\mathrm{soc}}, \end{aligned} \tag{39}$$

This expression defines a polynomial in x^{s}_1, where $x^{\mathrm{s}}_1 \in [0, 1]$ lies in a compact and convex domain. The cost function J_{soc} is continuous and differentiable on this interval, and reduces to a quadratic form. The leading coefficient of the quadratic term in Equation (39) is $K^{\mathrm{s}}_1 + K^{\mathrm{b}}_1 > 0$. Hence, J_{soc} is strictly convex over the domain of x^{s}_1. In Equation (6) and (24), $x^{\mathrm{s}}_1 = x^{\mathrm{s}}_{1,\mathrm{HDV}} + pq_{\mathrm{s}}$. As $x^{\mathrm{s}*}_{1,\mathrm{HDV}}$ is unique and p is given, ${q_{\mathrm{s}}}^*$ exists and is unique for a minimum value of J_{soc}.

Based on above convex analysis, J_{soc} has a global minimum point x_1^{s}, which we defined as $\mathbf{B}$:

$$\mathbf{B} = \frac{2K_2 - K_3 + K_4}{2(K_1 + K_2)}, \tag{40}$$

where we have $\mathbf{B} > \Phi$, as we define the social optimal scenario has higher steadfast proportion than HDV-only scenario.

Let's consider possible equilibrium cases (denoted as $\mathbf{x}^*$) at mixed autonomy scenario. Given CAV penetration rate p, there are 3 possible cases, which are: Case 1. $J_1^{\text{s}}(\mathbf{x}^*) = J_1^{\text{b}}(\mathbf{x}^*)$. Case 2. $J_1^{\text{s}}(\mathbf{x}^*) > J_1^{\text{b}}(\mathbf{x}^*)$. Case 3. $J_1^{\text{s}}(\mathbf{x}^*) < J_1^{\text{b}}(\mathbf{x}^*)$.

Case 1:

If $J_1^{\text{s}}(\mathbf{x}^*) = J_1^{\text{b}}(\mathbf{x}^*)$ exists: based on Equation (19) and (20) , together with $x_1^{\text{s}} + x_1^{\text{b}} = 1$, the optimal $x_1^{\text{s}*}$ is calculated as:

$$x_1^{\text{s}*} = \frac{K_1^{\text{b}} + B_1^{\text{b}} - B_1^{\text{s}}}{K_1^{\text{s}} + K_1^{\text{b}}}, \tag{41}$$

where is the same steadfast proportion as HDV-only equilibrium Φ. Thus, $x_1^{\text{s}*} = \Phi$ in this case, and $\Phi \in [0, \mathbf{B}]$.

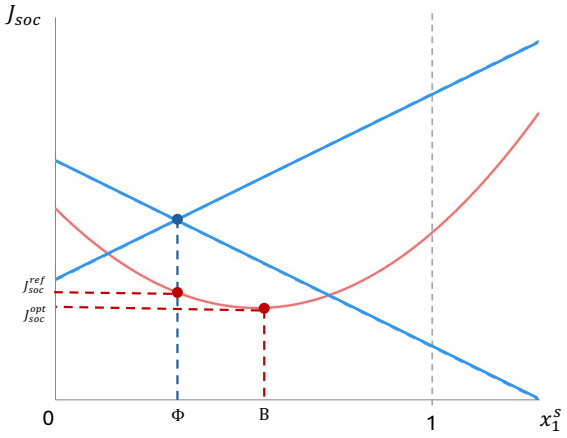

Figure 11: This figure shows three equilibrium cases for mixed autonomy scenario.

Based on Equation (24), the CAV proportion $x_{1,\text{CAV}}^{\text{s}} = pq_{\text{s}}$, and the corresponding HDV steadfast proportion $x_{1,\text{HDV}}^{\text{s}}$ can be updated as:

$$x_{1,\text{HDV}}^{\text{s}} = \Phi - pq_{\text{s}}, \tag{42}$$

Due to $x_{1,\text{HDV}}^{\text{s}} \in [0, 1-p]$, we have:

$$0 \leq \Phi - pq_{\text{s}} \leq 1 - p \tag{43}$$

As $\Phi < \mathbf{B}$, all CAV prefer steadfast to minimize J_{soc}. Therefore, under $q_{\text{s}}{}^* = 1$, Equation (43)

must hold. Since $\Phi \leq 1$ always holds, the admissible range of p that allows this case to occur is:

$$p \leq \Phi \tag{44}$$

Thus, when $0 \leq p \leq \Phi$, the equilibrium case satisfies $J_1^{\mathrm{s}}(\mathbf{x}^*) = J_1^{\mathrm{b}}(\mathbf{x}^*)$. When p increases, J_{soc} keeps invariant, and $J_{\mathrm{soc}} = J_{\mathrm{soc}}^{\mathrm{ref}}$.

Case 2:

If $J_1^{\mathrm{s}}(\mathbf{x}^*) > J_1^{\mathrm{b}}(\mathbf{x}^*)$ exists: ${x_{1,\mathrm{HDV}}^{\mathrm{s}}}^* = 0$. From Equation (6), it follows that ${x_{1,\mathrm{CAV}}^{\mathrm{s}}}^* = {x_1^{\mathrm{s}}}^*$. Based on Equation (19) and (20), together with $x_1^{\mathrm{s}} + x_1^{\mathrm{b}} = 1$, the optimal ${x_1^{\mathrm{s}}}^*$ satisfies:

$${x_1^{\mathrm{s}}}^* > \frac{K_1^{\mathrm{b}} + B_1^{\mathrm{b}} - B_1^{\mathrm{s}}}{K_1^{\mathrm{s}} + K_1^{\mathrm{b}}} = \Phi, \tag{45}$$

There are two possible minimum cases for J_{soc}: (1) $\Phi < {x_1^{\mathrm{s}}}^* < \mathbf{B}$, (2) ${x_1^{\mathrm{s}}}^* \geq \mathbf{B}$.

(1) $\Phi < {x_1^{\mathrm{s}}}^* < \mathbf{B}$. In this case, $x_1^{\mathrm{s}} = x_{1,\mathrm{CAV}}^{\mathrm{s}} = pq_{\mathrm{s}}$, and all CAV prefer steadfast, which means $q_{\mathrm{s}}^* = 1$, thus ${x_1^{\mathrm{s}}}^* = p$. Also, the range of p is updated to be $\Phi < p < \mathbf{B}$.

From Equation (39), J_{soc} can be updated to be a quadratic function of p, and the range of p is $\Phi < p < \mathbf{B}$. When $p \in (\Phi, \mathbf{B})$ increases, J_{soc} decreases.

(2) ${x_1^{\mathrm{s}}}^* \geq \mathbf{B}$. In this case, $x_1^{\mathrm{s}} = pq_{\mathrm{s}} \geq \mathbf{B}$. As the range of $x_1^{\mathrm{s}} \in [0, p]$, if this case exists, there must satisfy $p \geq \mathbf{B}$.

From Equation (39), J_{soc} is a quadratic function of x_1^{s}, and the range of $x_1^{\mathrm{s}} \geq \mathbf{B}$. J_{soc} always reach its minimum value at ${x_1^{\mathrm{s}}}^* = \mathbf{B}$. When $p \in [\mathbf{B}, 1]$ increases, J_{soc} keeps invariant.

Case 3:

If $J_1^{\mathrm{s}}(\mathbf{x}^*) < J_1^{\mathrm{b}}(\mathbf{x}^*)$ exists: $x_{1,\mathrm{HDV}}^{\mathrm{s}} = 1 - p$, and $x_1^{\mathrm{s}} = 1 - p + pq_{\mathrm{s}}$. Based on Equation (19) and (20), together with $x_1^{\mathrm{s}} + x_1^{\mathrm{b}} = 1$, the optimal ${x_1^{\mathrm{s}}}^*$ satisfies:

$${x_1^{\mathrm{s}}}^* < \frac{K_1^{\mathrm{b}} + B_1^{\mathrm{b}} - B_1^{\mathrm{s}}}{K_1^{\mathrm{s}} + K_1^{\mathrm{b}}} = \Phi, \tag{46}$$

Since $x_1^{\mathrm{s}} < \Phi$, all CAV prefer steadfast, thus $q_{\mathrm{s}} = 1$. Also, we have $1 - p + pq_{\mathrm{s}} < \Phi$, thus $\Phi > 1$. This contradicts the range of $\Phi < \mathbf{B} \leq 1$, so this case does not exists.

In conclusion, combined Case 1, Case 2, and Case 3: in $0 \leq p \leq \mathbf{A}$, when p increases, ${x_1^{\mathrm{s}}}^* = \Phi$, J_{soc} keep invariant. In $\Phi < p < \mathbf{B}$, when p increases, J_{soc} decreases. In $\mathbf{B} \leq p \leq 1$, when p increases, J_{soc} reaches the global minimum point and keep invariant.

□

9.4 Proof for Theorem 3

Proof. All CAV and HDV types are described as j in the mixed autonomy scenario, which we have a disjoint union $\mathcal{J} = \mathcal{H} \cup \mathcal{C}$. Based on Equations (31) and (32), and noting that the total steadfast proportion is given by $x_1^{\mathrm{s}} = \sum_{j \in \mathcal{J}} x_{1,j}^{\mathrm{s}}$, i.e., the aggregate steadfast ratio equals the sum of the

steadfast proportions of all vehicle types, we can reformulate the equations as follows:

$$\tilde{J}^{\mathrm{s}}_{1,j}(\mathbf{x}) = cos(\theta_j)J^{\mathrm{s}}_1(\mathbf{x}) + sin(\theta_j)\frac{\partial J_{\mathrm{soc}}(\mathbf{x})}{\partial x^{\mathrm{s}}_1}\frac{\partial}{\partial x^{\mathrm{s}}_{1,j}}\sum_{j=1}^{J} x^{\mathrm{s}}_{1,j}, \tag{47}$$

$$= (cos(\theta_j) + 2sin(\theta_j))K^{\mathrm{s}}_1 x^{\mathrm{s}}_1 + cos(\theta_j)B^{\mathrm{s}}_1 + sin(\theta_j)(B^{\mathrm{s}}_1 + n^{\mathrm{exit}}_2 K^{\mathrm{exit}}_2 + n^{\mathrm{enter}}_0 K^{\mathrm{enter}}_0), \tag{48}$$

$$\tilde{J}^{\mathrm{b}}_{1,j}(\mathbf{x}) = cos(\theta_j)J^{\mathrm{b}}_1(\mathbf{x}) + sin(\theta_j)\frac{\partial J_{\mathrm{soc}}(\mathbf{x})}{\partial x^{\mathrm{b}}_1}\frac{\partial}{\partial x^{\mathrm{b}}_{1,j}}\sum_{j=1}^{J} x^{\mathrm{b}}_{1,j}, \tag{49}$$

$$= (cos(\theta_j) + 2sin(\theta_j))K^{\mathrm{b}}_1 x^{\mathrm{b}}_1 + cos(\theta_j)B^{\mathrm{b}}_1 + sin(\theta_j)(B^{\mathrm{b}}_1 + n^{\mathrm{s}}_2 K^{\mathrm{s}}_2), \tag{50}$$

Since $x^{\mathrm{s}}_1 = \sum_j x^{\mathrm{s}}_{1,j}$, we have $\frac{\partial x^{\mathrm{s}}_1}{\partial x^{\mathrm{s}}_{1,j}}$, hence $\frac{\partial J_{\mathrm{soc}}}{\partial x^{\mathrm{s}}_{1,j}} = \frac{\partial J_{\mathrm{soc}}}{\partial x^{\mathrm{s}}_1}$. Same for x^{b}_1. Therefore, we have the fact that $\frac{\partial}{\partial x^{\mathrm{s}}_{1,j}}\sum_{j=1}^{J} x^{\mathrm{s}}_{1,j} = 1$ and $\frac{\partial}{\partial x^{\mathrm{b}}_{1,j}}\sum_{j=1}^{J} x^{\mathrm{b}}_{1,j} = 1$.

Also, we can simplify Equation (48) and (50) as:

$$\tilde{J}^{\mathrm{s}}_{1,j} = K^{\mathrm{s}}_{1,j}x^{\mathrm{s}}_1 + B^{\mathrm{s}}_{1,j}, \tag{51}$$

$$\tilde{J}^{\mathrm{b}}_{1,j} = K^{\mathrm{b}}_{1,j}x^{\mathrm{b}}_1 + B^{\mathrm{b}}_{1,j}. \tag{52}$$

where $K^{\mathrm{s}}_{1,j} := (cos(\theta_j) + 2sin(\theta_j))K^{\mathrm{s}}_1$, $B^{\mathrm{s}}_{1,j} := cos(\theta_j)B^{\mathrm{s}}_1 + sin(\theta_j)(B^{\mathrm{s}}_1 + n^{\mathrm{exit}}_2 K^{\mathrm{exit}}_2 + n^{\mathrm{enter}}_0 K^{\mathrm{enter}}_0)$, $K^{\mathrm{b}}_{1,j} := (cos(\theta_j) + 2sin(\theta_j))K^{\mathrm{b}}_1$, and $B^{\mathrm{b}}_{1,j} := cos(\theta_j)B^{\mathrm{b}}_1 + sin(\theta_j)(B^{\mathrm{b}}_1 + n^{\mathrm{s}}_2 K^{\mathrm{s}}_2)$.

We define $\Delta_j(x^{\mathrm{s}}_1) = \tilde{J}^{\mathrm{s}}_{1,j} - \tilde{J}^{\mathrm{b}}_{1,j}$, which represents the cost difference between choosing steadfast and the bypass for vehicle type j. Since the total proportion on the two behaviors satisfies $x^{\mathrm{s}}_1 + x^{\mathrm{b}}_1 = 1$, we can substitute $x^{\mathrm{b}}_1 = 1 - x^{\mathrm{s}}_1$ into the above expression. Thus, $\Delta_j(x^{\mathrm{s}}_1)$ becomes a function of x^{s}_1 only and can be written in the following linear form:

$$\Delta_j(x^{\mathrm{s}}_1) = (K^{\mathrm{s}}_{1,j} + K^{\mathrm{b}}_{1,j})x^{\mathrm{s}}_1 + B^{\mathrm{s}}_{1,j} - B^{\mathrm{b}}_{1,j} - K^{\mathrm{b}}_{1,j}. \tag{53}$$

Since $\theta_j \in (-arctan\frac{1}{2}, \pi - arctan\frac{1}{2})$, we have $cos(\theta_j) + 2sin(\theta_j) > 0$. Under this condition, for any vehicle type j, $J^{\mathrm{s}}_{1,j}$ is monotonically increasing in x^{s}_1, whereas $J^{\mathrm{b}}_{1,j}$ is monotonically decreasing in x^{s}_1. Assume there exists type j's equilibrium $\tilde{J}^{\mathrm{s}}_{1,j}(\chi_j) = \tilde{J}^{\mathrm{b}}_{1,j}(\chi_j)$, and we define the total steadfast proportion x^{s}_1 at such equilibrium is χ_j:

$$\chi_j = \frac{B^{\mathrm{b}}_{1,j} + K^{\mathrm{b}}_{1,j} - B^{\mathrm{s}}_{1,j}}{K^{\mathrm{s}}_{1,j} + K^{\mathrm{b}}_{1,j}} \tag{54}$$

For the true $x^{\mathrm{s}*}_1$ under penetration p, vehicle type j can only fall into one of the following three cases:

- If $x^{\mathrm{s}*}_1 < \chi_j$, we have $\tilde{J}^{\mathrm{s}}_{1,j} < \tilde{J}^{\mathrm{b}}_{1,j}$, type j strictly keeps steadfast ($x^{\mathrm{s}}_{1,j} = w_j(p)$).
- If $x^{\mathrm{s}*}_1 > \chi_j$, we have $\tilde{J}^{\mathrm{s}}_{1,j} > \tilde{J}^{\mathrm{b}}_{1,j}$, type j strictly keeps bypass ($x^{\mathrm{s}}_{1,j} = 0$).
- If $x^{\mathrm{s}*}_1 = \chi_j$, we have $\tilde{J}^{\mathrm{s}}_{1,j} = \tilde{J}^{\mathrm{b}}_{1,j}$, type j is indifferent between two choices.

Since all vehicle types are distinct and each type has a typical θ_j, which means each vehicle type has a unique threshold χ_j. Then we rank all thresholds χ_j in ascending order:

$$\chi_1 < \chi_2 < \cdots < \chi_J. \tag{55}$$

In any Wardrop equilibrium, there exists an index k such that:

- all types with threshold $> \chi_k$ are fully steadfast.
- all types with threshold $< \chi_k$ are fully bypass.
- only type k may mix (if $x_1^{\mathrm{s}*} = \chi_k$).

Check the monotonicity of $W_k(p)$ for p under fixed k.

Define total steadfast proportion tail sums other than vehicle k as $W_k(p)$ for $k = 1, \cdots, J$:

$$W_k(p) = \sum_{j \in \mathcal{H}, \chi_j > \chi_k} (1-p) w_h^{\mathrm{HDV}} + \sum_{j \in \mathcal{C}, \chi_j > \chi_k} p w_c^{\mathrm{CAV}} \tag{56}$$

When k is fixed, Equation (56) is affine in p. Let

$$A_k := \sum_{j \in \mathcal{C}, \chi_j > \chi_k} w_c^{\mathrm{CAV}} - \sum_{j \in \mathcal{H}, \chi_j > \chi_k} w_h^{\mathrm{HDV}}.$$

Then $W_k(p)$ has slope A_k with respect to p. Therefore, $W_k(p)$ is increasing, constant, or decreasing in p if $A_k > 0$, $A_k = 0$, or $A_k < 0$, respectively.

Check the monotonicity of J_{soc} for p under fixed k.

Under fixed vehicle type k, the total steadfast proportion $x_1^{\mathrm{s}*} = \chi_k$, which is fixed. According to Equation (39), the social cost J_{soc} depends only on x_1^{s}. As a result, J_{soc} remains constant within the region where the vehicle type k is fixed. Consequently, variations in J_{soc} occur only at the switching points where the fixed vehicle type k changes.

Classify type k's behavior.

When k is fixed, there are exactly two behavior regimes for vehicle type k:

Regime 1: Interior Regime for Mixed type k. When vehicle type k satisfy:

$$0 < \chi_k - W_k(p) < w_k(p), \tag{57}$$

Vehicle type k adopts a mixed strategy and is partially steadfast and partially bypass (Figure 12a). Vehicle types with $\chi_j > \chi_k$ are fully steadfast, while vehicle types with $\chi_j < \chi_k$ are fully bypass.

Regime 2: Boundary Regime for Purely type k. When vehicle type k satisfy:

$$\chi_k - W_k(p) = 0, \tag{58}$$

vehicle type k becomes purely bypass (i.e., $x_{1,k}^s = 0$). Vehicle types with $\chi_j > \chi_k$ are fully steadfast, while vehicle types with $\chi_j \leq \chi_k$ are fully bypass. This boundary corresponds to the transition from

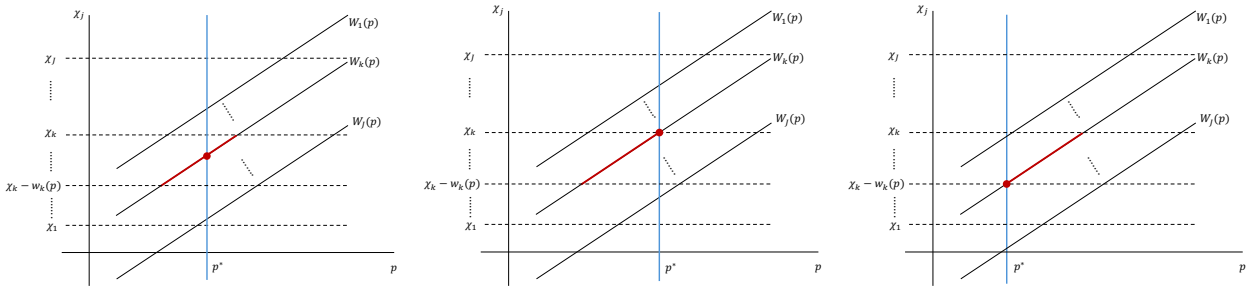

(a) Mixed type k (b) Purely type k bypass (c) Purely type k steadfast

Figure 12: These figures show type k's behavior regimes.

the regime where type k is mixed to the regime where type $k+1$ becomes the potentially mixed type.

When vehicle type k satisfy:

$$\chi_k - W_k(p) = w_k(p), \tag{59}$$

vehicle type k becomes purely steadfast (i.e., $x^s_{1,k} = w_k(p)$). Vehicle types with $\chi_j \geq \chi_k$ are fully steadfast, while vehicle types with $\chi_j < \chi_k$ are fully bypass. In this case, the system transitions to the regime associated with type $k-1$.

Check the regime pairwise disjointness of $k-1$ and $k+1$.

Based on definition of 56, we have $W_{k-1}(p) = W_k(p) + w_k(p)$ and $W_{k+1}(p) = W_k(p) - w_{k+1}(p)$. Since $p \in I_k$, $W_k(p) < \chi_k < W_k(p) + w_k(p)$.

For $k-1$:

$$W_{k-1}(p) = W_k(p) + w_k(p) > \chi_k > \chi_{k-1}, \tag{60}$$

thus there does not exist $p \in I_{k-1}$.

For $k+1$:

$$W_{k+1}(p) + w_{k+1}(p) = W_k(p) < \chi_k < \chi_{k+1}, \tag{61}$$

thus there does not exist $p \in I_{k+1}$.

In conclusion, the neighboring regime will not overlap with each other.

Check exact range of p under I_k.

Based on (57), we can get the current range of p. If $A_k > 0$:

$$\frac{\chi_k - \sum_{j\in\mathcal{H},\chi_j>\chi_k} w_h^{\mathrm{HDV}}}{w_{c=k}^{\mathrm{CAV}} + A_k} < p < \frac{\chi_k - \sum_{j\in\mathcal{H},\chi_j>\chi_k} w_h^{\mathrm{HDV}}}{A_k}. \tag{62}$$

If $A_k < 0$, only when $w_{c=k}^{\text{CAV}} + A_k \geq 0$, we have:

$$p > \frac{\chi_k - \sum_{j \in \mathcal{H}, \chi_j > \chi_k} w_h^{\text{HDV}}}{A_k}. \tag{63}$$

If $A_k = 0$, we have:

$$p > \frac{\chi_k - \sum_{j \in \mathcal{H}, \chi_j > \chi_k} w_h^{\text{HDV}}}{w_{c=k}^{\text{CAV}} + A_k}. \tag{64}$$

□

References

Adebisi, A., Liu, Y., Schroeder, B., Ma, J., Cesme, B., Jia, A., and Morgan, A. (2020). Developing highway capacity manual capacity adjustment factors for connected and automated traffic on freeway segments. *Transportation Research Record*, 2674(10):401–415.

Ao, D., Lai, Z., and Li, S. (2024). Control of dynamic ride-hailing networks with a mixed fleet of autonomous vehicles and for-hire human drivers. *Transportation Research Part E: Logistics and Transportation Review*, 189:103680.

Başar, T. and Olsder, G. J. (1999). *Dynamic Noncooperative Game Theory*. SIAM.

Beckmann, M., McGuire, C. B., and Winsten, C. B. (1956). Studies in the economics of transportation. Technical report.

Cassidy, M. J. and Bertini, R. L. (1999). Some traffic features at freeway bottlenecks. *Transportation Research Part B: Methodological*, 33(1):25–42.

Chandra, R. and Manocha, D. (2022). Gameplan: Game-theoretic multi-agent planning with human drivers at intersections, roundabouts, and merging. *IEEE Robotics and Automation Letters*, 7(2):2676–2683.

Chen, D. and Ahn, S. (2018). Capacity-drop at extended bottlenecks: Merge, diverge, and weave. *Transportation Research Part B: Methodological*, 108:1–20.

Chen, D., Ahn, S., Chitturi, M., and Noyce, D. A. (2017a). Towards vehicle automation: Roadway capacity formulation for traffic mixed with regular and automated vehicles. *Transportation research part B: methodological*, 100:196–221.

Chen, Z., He, F., Yin, Y., and Du, Y. (2017b). Optimal design of autonomous vehicle zones in transportation networks. *Transportation Research Part B: Methodological*, 99:44–61.

Chiou, S.-W. (2005). Bilevel programming for the continuous transport network design problem. *Transportation Research Part B: Methodological*, 39(4):361–383.

Dresner, K. and Stone, P. (2008). A multiagent approach to autonomous intersection management. *Journal of artificial intelligence research*, 31:591–656.

Du, R., Chen, S., Li, Y., Dong, J., Ha, P. Y. J., and Labi, S. (2020). A cooperative control framework for cav lane change in a mixed traffic environment. *arXiv preprint arXiv:2010.05439*.

Fan, T., Chen, J., and Chung, E. (2025). Integrating micro and macro traffic control for mixed autonomy traffic. *Communications in Transportation Research*, 5:100188.

Ghiasi, A., Hussain, O., Qian, Z. S., and Li, X. (2017). A mixed traffic capacity analysis and lane management model for connected automated vehicles: A markov chain method. *Transportation Research Part B: Methodological*, 106:266–292.

Gipps, P. G. (1986). A model for the structure of lane-changing decisions. *Transportation Research Part B: Methodological*, 20(5):403–414.

Guo, Q., Ban, X. J., and Aziz, H. A. (2021). Mixed traffic flow of human driven vehicles and automated vehicles on dynamic transportation networks. *Transportation research part C: emerging technologies*, 128:103159.

Guo, Y. and Ma, J. (2020). Leveraging existing high-occupancy vehicle lanes for mixed-autonomy traffic management with emerging connected automated vehicle applications. *Transportmetrica A: Transport Science*, 16(3):1375–1399.

Guo, Z., Wang, D. Z., and Wang, D. (2022). Managing mixed traffic with autonomous vehicles–a day-to-day routing allocation scheme. *Transportation research part C: emerging technologies*, 140:103726.

Hidas, P. (2002). Modelling lane changing and merging in microscopic traffic simulation. *Transportation Research Part C: Emerging Technologies*, 10(5-6):351–371.

Ji, A. and Levinson, D. (2020). A review of game theory models of lane changing. *Transportmetrica A: transport science*, 16(3):1628–1647.

Kita, H. (1999). A merging–giveway interaction model of cars in a merging section: a game theoretic analysis. *Transportation Research Part A: Policy and Practice*, 33(3-4):305–312.

Kita, H., Tanimoto, K., and Fukuyama, K. (2002). A game theoretic analysis of merging-giveway interaction: a joint estimation model. In *Transportation and Traffic Theory in the 21st Century: Proceedings of the 15th International Symposium on Transportation and Traffic Theory, Adelaide, Australia, 16-18 July 2002*, pages 503–518. Emerald Group Publishing Limited.

Krajzewicz, D., Erdmann, J., Behrisch, M., and Bieker, L. (2012). Recent development and applications of SUMO - Simulation of Urban MObility. *International Journal On Advances in Systems and Measurements*, 5(3&4):128–138.

Laval, J. A. and Daganzo, C. F. (2006). Lane-changing in traffic streams. *Transportation Research Part B: Methodological*, 40(3):251–264.

Laval, J. A. and Leclercq, L. (2008). Microscopic modeling of the relaxation phenomenon using a macroscopic lane-changing model. *Transportation Research Part B: Methodological*, 42(6):511–522.

Lazar, D. A., Coogan, S., and Pedarsani, R. (2017). Capacity modeling and routing for traffic networks with mixed autonomy. In *Decision and Control (CDC), 2017 IEEE 56th Conference on, to appear, IEEE*.

Lazar, D. A., Coogan, S., and Pedarsani, R. (2018). The price of anarchy for transportation networks with mixed autonomy. In *2018 Annual American Control Conference (ACC)*, pages 6359–6365. IEEE.

Lee, J. and Cassidy, M. J. (2008). An empirical and theoretical study of freeway weave bottlenecks.

Li, A., Armijos, A. S. C., and Cassandras, C. G. (2023). Cooperative lane changing in mixed traffic can be robust to human driver behavior. In *2023 62nd IEEE Conference on Decision and Control (CDC)*, pages 5123–5128. IEEE.

Li, R., Brown, P. N., and Horowitz, R. (2021). Employing altruistic vehicles at on-ramps to improve the social traffic conditions. In *2021 American Control Conference (ACC)*, pages 4547–4552. IEEE.

Li, R., Liu, J., and Horowitz, R. (2020a). A game-theoretic model for aggregate lane choice behavior of highway mainline vehicles at the vicinity of on-ramps. In *2020 American Control Conference (ACC)*, pages 5376–5381.

Li, R., Liu, J., and Horowitz, R. (2020b). A game-theoretic model for aggregate lane choice behavior of highway mainline vehicles at the vicinity of on-ramps. In *2020 American Control Conference (ACC)*, pages 5376–5381. IEEE.

Li, R., Liu, X., and Nie, Y. M. (2018). Managing partially automated network traffic flow: Efficiency vs. stability. *Transportation Research Part B: Methodological*, 114:300–324.

Li, R., Mehr, N., and Horowitz, R. (2019). An extended game–theoretic model for aggregate lane choice behavior of vehicles at traffic diverges with a bifurcating lane. In *2019 IEEE Intelligent Transportation Systems Conference (ITSC)*, pages 2226–2231. IEEE.

Liebrand, W. B., Wilke, H. A., Vogel, R., and Wolters, F. J. (1986). Value orientation and conformity: A study using three types of social dilemma games. *Journal of Conflict Resolution*, 30(1):77–97.

Lioris, J., Pedarsani, R., Tascikaraoglu, F. Y., and Varaiya, P. (2017). Platoons of connected vehicles can double throughput in urban roads. *Transportation Research Part C: Emerging Technologies*, 77:292–305.

Lopez, V. G., Lewis, F. L., Liu, M., Wan, Y., Nageshrao, S., and Filev, D. (2022). Game-theoretic lane-changing decision making and payoff learning for autonomous vehicles. *IEEE Transactions on Vehicular Technology*, 71(4):3609–3620.

Luo, Z.-Q., Pang, J.-S., and Ralph, D. (1996). *Mathematical programs with equilibrium constraints*. Cambridge University Press.

Marczak, F., Leclercq*, L., and Buisson, C. (2015). A macroscopic model for freeway weaving sections. *Computer-Aided Civil and Infrastructure Engineering*, 30(6):464–477.

Mehr, N., Li, R., and Horowitz, R. (2021). A game theoretic macroscopic model of lane choices at traffic diverges with applications to mixed–autonomy networks. *Transportation Research Part B: Methodological*, 144:45–59.

Outrata, J., Kocvara, M., and Zowe, J. (2013). *Nonsmooth approach to optimization problems with equilibrium constraints: theory, applications and numerical results*, volume 28. Springer Science & Business Media.

Rios-Torres, J. and Malikopoulos, A. A. (2016). A survey on the coordination of connected and automated vehicles at intersections and merging at highway on-ramps. *IEEE Transactions on Intelligent Transportation Systems*, 18(5):1066–1077.

Rodrigues, M., McGordon, A., Gest, G., and Marco, J. (2018). Autonomous navigation in interaction-based environments—a case of non-signalized roundabouts. *IEEE Transactions on Intelligent Vehicles*, 3(4):425–438.

Roughgarden, T. and Tardos, É. (2002). How bad is selfish routing? *Journal of the ACM (JACM)*, 49(2):236–259.

Shalev-Shwartz, S., Shammah, S., and Shashua, A. (2016). Safe, multi-agent, reinforcement learning for autonomous driving. *arXiv preprint arXiv:1610.03295*.

Shladover, S. E., Su, D., and Lu, X.-Y. (2012). Impacts of cooperative adaptive cruise control on freeway traffic flow. *Transportation Research Record*, 2324(1):63–70.

Stern, R. E., Cui, S., Delle Monache, M. L., Bhadani, R., Bunting, M., Churchill, M., Hamilton, N., Haulcy, R., Pohlmann, H., Wu, F., et al. (2018). Dissipation of stop-and-go waves via control of autonomous vehicles: Field experiments. *Transportation research part C: emerging technologies*, 89:205–221.

Sun, D. and Elefteriadou, L. (2010). Research and implementation of lane-changing model based on driver behavior. *Transportation Research Record*, 2161(1):1–10.

Talebpour, A. and Mahmassani, H. S. (2016). Influence of connected and autonomous vehicles on traffic flow stability and throughput. *Transportation research part C: emerging technologies*, 71:143–163.

Talebpour, A., Mahmassani, H. S., and Hamdar, S. H. (2015). Modeling lane-changing behavior in a connected environment: A game theory approach. *Transportation Research Part C: Emerging Technologies*, 59:216–232.

Toledo, T., Koutsopoulos, H. N., and Ben-Akiva, M. E. (2003). Modeling integrated lane-changing behavior. In *Transportation Research Record: Journal of the Transportation Research Board, Volume: 1857 issue: 1*, pages 30–38.

Transportation Research Board (2010). *Highway Capacity Manual*. Transportation Research Board, National Research Council, Washington, D.C., 5th ed. edition.

Treiber, M. and Kesting, A. (2013). *Traffic flow dynamics*, volume 1. Springer.

Van Lange, P. A. (1999). The pursuit of joint outcomes and equality in outcomes: an integrative model of social value orientation. *Journal of personality and social psychology*, 77(2):337.

Vinitsky, E., Kreidieh, A., Le Flem, L., Kheterpal, N., Jang, K., Wu, C., Wu, F., Liaw, R., Liang, E., and Bayen, A. M. (2018). Benchmarks for reinforcement learning in mixed-autonomy traffic. In *Conference on robot learning*, pages 399–409. PMLR.

Wang, J., Zhang, Q., Zhao, D., and Chen, Y. (2019). Lane change decision-making through deep reinforcement learning with rule-based constraints. In *2019 International Joint Conference on Neural Networks (IJCNN)*, pages 1–6. IEEE.

Wang, J., Zheng, Y., Xu, Q., Wang, J., and Li, K. (2020). Controllability analysis and optimal control of mixed traffic flow with human-driven and autonomous vehicles. *IEEE Transactions on Intelligent Transportation Systems*, 22(12):7445–7459.

Wardrop, J. G. (1952). Some theoretical aspects of road traffic research. In *Proceedings of the Institution of Civil Engineers, Volume 1 Issue 3*, pages 325–362.

Wu, C., Kreidieh, A., Vinitsky, E., and Bayen, A. M. (2017). Emergent behaviors in mixed-autonomy traffic. In *Conference on Robot Learning*, pages 398–407.

Wu, M., Wang, X., Yin, Y., Liu, H., Wang, B., and Lynch, J. P. (2023). Leveraging connected and automated vehicles for participatory traffic control. Technical report.

Yan, L., Liang, J., and Yang, K. (2024). Bi-level control of weaving sections in mixed traffic environments with connected and automated vehicles. *arXiv preprint arXiv:2403.16225*.

Zhang, K. and Nie, Y. M. (2018). Mitigating the impact of selfish routing: An optimal-ratio control scheme (orcs) inspired by autonomous driving. *Transportation Research Part C: Emerging Technologies*, 87:75–90.

Zhou, M., Qu, X., and Jin, S. (2016). On the impact of cooperative autonomous vehicles in improving freeway merging: a modified intelligent driver model-based approach. *IEEE Transactions on Intelligent Transportation Systems*, 18(6):1422–1428.